12-14-2013

Temperature Effects of Dielectric Properties and their Impact on Medical Device Development

Erin Elizabeth Colebeck

Temperature effects of dielectric properties and their impact on medical device development

By

Erin Colebeck

A Thesis
Submitted to the Faculty of
Mississippi State University
in Partial Fulfillment of the Requirements
for the Degree of Master of Science
in Biomedical Engineering
in the Department of Agriculture and Biological Engineering

Mississippi State, Mississippi

December 2013

Temperature effects of dielectric properties and their impact on medical device development

By

Erin Colebeck

Approved:

_____

Erdem Topsakal
(Director of Thesis)

_____

Jun Liao
(Committee Member)

_____

Robert C. Cooper
(Committee Member)

_____

Steven H. Elder
(Committee Member/Graduate Coordinator)

_____

Achille Messac
Dean
Bagley College of Engineering

Name: Erin Colebeck

Date of Degree: December 14, 2013

Institution: Mississippi State University

Major Field: Biomedical Engineering

Director of Thesis: Dr. Erdem Topsakal

Title of Study: Temperature effects of dielectric properties and their impact on medical device development

Pages in Study: 56

Candidate for Degree of Master of Science

Dielectric properties play an influential role in the development of medical devices. Understanding the behavior of these properties and how they respond to external stimuli, such as heat, over an extended frequency has yet to be researched. The focus of this study is to examine the impact of temperature on dielectric properties from 500 MHz to 10 GHz in order to better match the antenna properties of medical applications to the dielectric properties of biological tissue in question; more specifically, microwave ablation, microwave hyperthermia, and thermal modeling of brown adipose tissue's metabolic processes.

The dielectric properties of biological tissue samples from porcine lung, liver, heart, skin, fat, and muscle as well as brown adipose tissue and white adipose tissue from rat have been tested. These results have then been used to develop medical applications involving microwave antennas.

Keywords: dielectric properties, medical applications, microwave antennas

TABLE OF CONTENTS

LIST OF TABLES

LIST OF FIGURES

CHAPTER I

INTRODUCTION

The electrical properties of biological tissue play an important role in understanding and developing new biomedical applications in the field of electromagnetics. Current fields of study include, but are not limited to pulmonary edema, chemo-thermotherapy for breast cancer, microwave ablation, metabolic processes of brown adipose tissue, in vitro cell culture, and implantable medical devices [1-6]. While the basic understanding of these properties has been researched and reviewed for well over a century, precise details concerning the manipulation of parameters (such as heating, changing the frequency, etc.) have come into question. Defining these results will allow for a better understanding of the properties when manipulation occurs, leading to an increased development of electromagnetic and microwave medical applications.

It is well understood that the electrical properties determine the direction and pathways of current flow throughout the body. When a tissue is responding to electrical stimulation, data is needed on the specific conductivity and relative permittivity of that tissue [7-9]. Currently, the electrical properties of any material, including biological tissues, can be divided into two main categories: conducting and insulating. If the material is categorized as a conductor, the electrical charges move freely once an electric field has been introduced. If the material has been specified as an insulator, the charges are fixed and unable to move freely [9].

If a conductor is placed in an electric field, charges will move within the conductor until the interior field is zero. For an insulator, free charges do not exist so net migration of the charge does not occur. Polarization can occur when a polar material is exposed to an applied electric field. The field orients the dipoles within the material, along with the relatively free charges that most materials contain, and the electric field inside the material is reduced to its free space value. If the material is an insulator, the net field inside the material is significantly lowered relative to the applied field. If the material is a good conductor, it is effectively zero [7]. The dielectric properties are related to the dielectric losses or reduction associated with the relaxation of electric dipoles. Each dispersion is characterized by an average relaxation time defined by the factor ε_r, relative permittivity or dielectric constant [10]. Relative permittivity is a complex quantity made of real and imaginary components and explained by the following equation:

$$\varepsilon_r = \varepsilon' - i\varepsilon'' \tag{1.1}$$

where ε' is the relative permittivity of the material, ε_r is the complex relative permittivity, and ε'' is the out of phase loss factor and is associated such that

$$\varepsilon'' = \sigma/\varepsilon_0\omega \tag{1.2}$$

where σ is the total conductivity of the material. Here ε_0 is the permittivity of free space and ω is the angular frequency of the field [11].

At the molecular level, electromagnetic radiation causes dispersions, a decrease in relative permittivity in three main divisions known as α, β and γ as seen in Figure 1. Dispersions relate to the orientation of the dipoles and motion of the free charges. The α dispersion occurs at low frequencies and is associated with the ionic diffusion processes

at the site of the cellular membrane. Polarization occurs, trapping freely charged particles at the internal membranes causing permittivity to be extremely high. Because of this, biological tissue is essentially conductive at these low frequencies. The β dispersion, which occurs in the kilohertz regions, is because of the polarization of cellular membranes which act as barriers to the passive flow of ions between the outer and inner cellular media. At this frequency range, the reactance of the membrane capacitance short-circuits the membrane resistance. This will allow the external electric field to penetrate into the cell interior [7, 12-13]. β dispersion can also be caused by polarization of proteins and other organic macromolecules. The γ dispersion, occurring in the gigahertz region, is because of the polarization of water molecules [8, 14-16]. Figure 1.1 depicts the occurrences of the three main dispersions. Outlined in red, this experimental data will involve testing biological tissue in the frequency range of 500 MHz to 10 GHz.

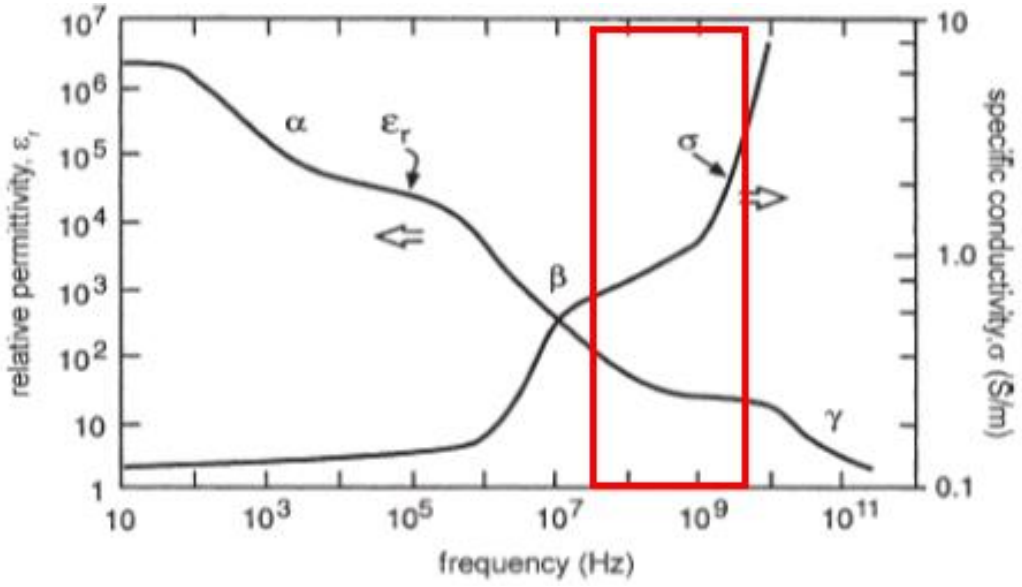

Figure 1.1 Dispersion of Biological Tissues [7]

CHAPTER II

ELECTRICAL PROPERTIES OF BIOLOGICAL TISSUE

2.1 Materials and Methods

In order to obtain results similar in dielectric properties to that of human tissue, porcine skin, fat, muscle, lung, liver, and heart were chosen [17]. The fresh samples were acquired from a local slaughter house and were all tested within 3 hours of animal death in order to maintain similar properties to that of *in vivo* testing using the Agilent Network Analyzer and slim probe kit.

The dielectric probe kit contains three different probe designs: performance, high temperature, and slim form. The performance probe kit, shown in Figure 2.1(a), functions over a frequency range of 500 MHz to 50 GHz and tolerates a temperature range of -40°C to 200°C. This extensive operating temperature range allows for dielectric measurements to be mapped against both frequency and temperature. The probe can be autoclaved, so it is useful in a variety of applications including food, medical, and chemical industries. The high temperature probe kit, shown in Figure 2.1(b), works over a frequency range of 200 MHz to 50 GHz and also tolerates a of -40°C to 200°C. This probe also measures the dielectric properties versus both frequency and temperature and it is resistant to corrosive or abrasive materials. Its wide brim allows for accurate measurements of flat surfaced solids or liquids. The slim probe kit, shown in Figure 2.1(c), is responsible for all of the testing done on biological tissue for this thesis. It operates over a frequency

range of 500 MHz to 50 GHz and tolerates a temperature range of 0°C to 125°C. To perform the measurements, this probe is either immerged in a liquid or placed on the surface of a material. For accurate measurements, a precise cut was made into the tissue and the tip of the probe made full contact with the exposed tissue.

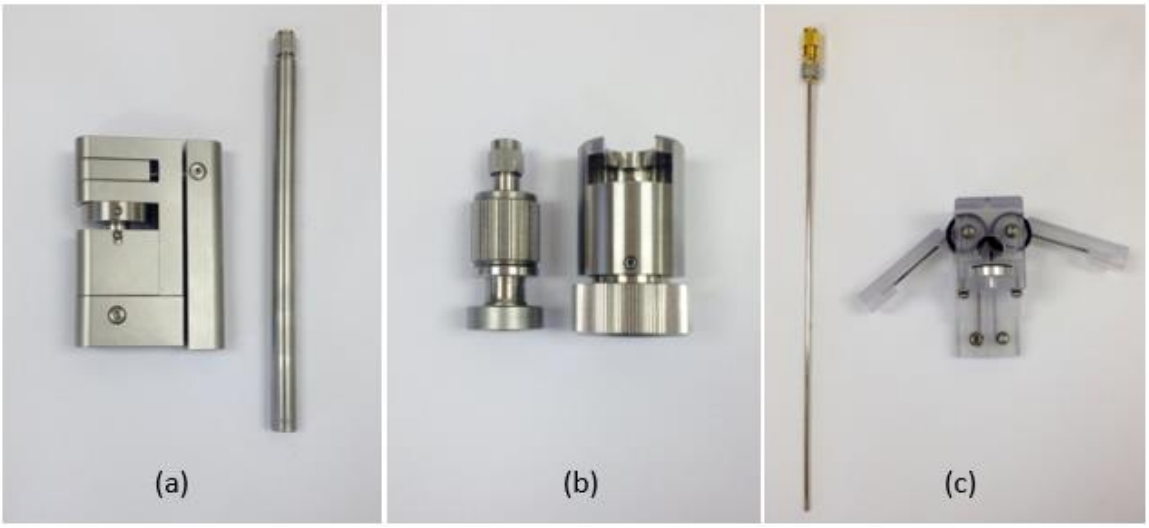

Figure 2.1 Performance Probe, (b) High Temperature Probe, and (c) Slim Probe

Before the tissues properties can be measured, the probe must be calibrated. This improves the accuracy of the measurements by removing any systematic errors that may occur. The main sources of error that can affect accuracy of the measurements of the sample can be: air bubbles in the sample or at the tip of the probe, the stability of the cable, air gaps between the material and the probe, or the dimensions of the sample. During calibration, three known standards are measured to compensate for these systematic errors: air, short circuit, and de-ionized water. Calibration is performed in

every study before taking each measurement of each tissue sample. The calibration set-up is shown in Figure 2.2.

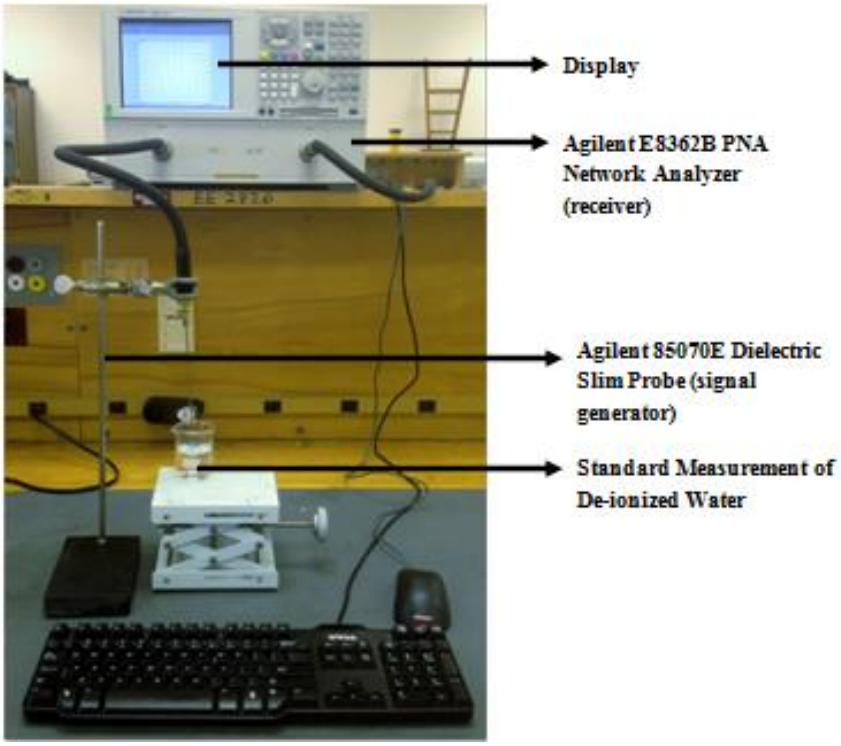

Figure 2.2 PNA Network Analyzer and Dielectric Slim Probe Kit Calibration Set-Up

The network analyzer measures the electrical signal reflection and signal transmission of each biological tissue. Biological tissues absorb power through the radiation of electrical signals. The network analyzer allows for these measurements to be mapped. A fiber optic temperature sensor (FISO Technologies Inc, Quebec, Canada) was used to monitor change in temperature for accurate dielectric property readings. Calibrations were made and the fiber optic temperature sensor was tested against an IKA® ETS D5 temperature sensor to provide accurate temperature readings of the tissue.

The fresh samples were at room temperature as seen in figures 2.3 and 2.4. Using the Agilent Network Analyzer and slim probe kit they were tested to gain standard dielectric property measurements of the porcine tissue at measured temperatures of 25˚C.

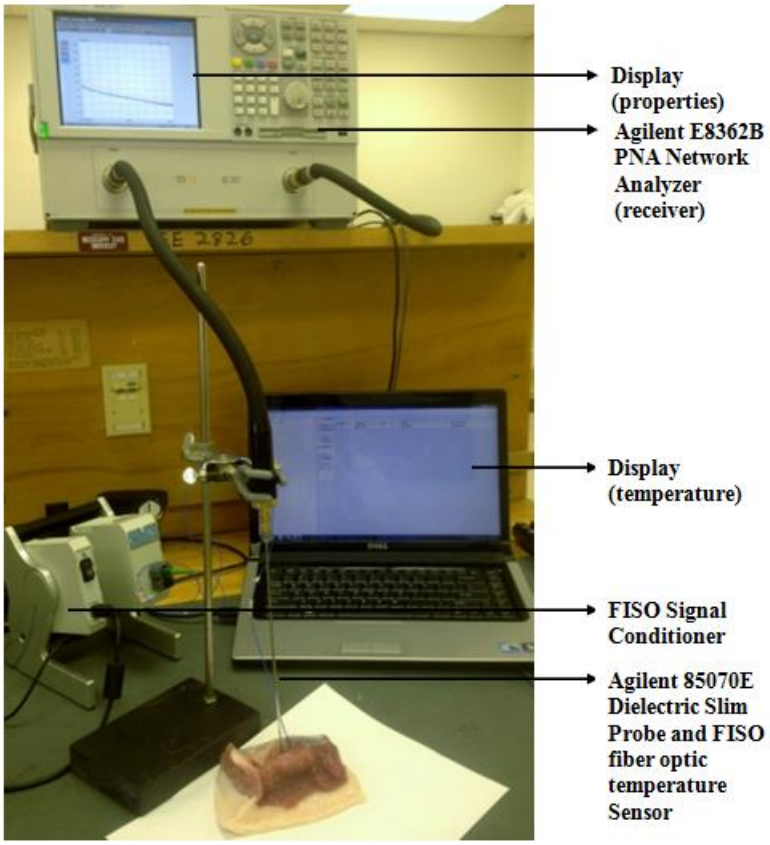

Figure 2.3 FISO Temperature Sensor, Agilent Network Analyzer, and Slim Probe Kit Set-up

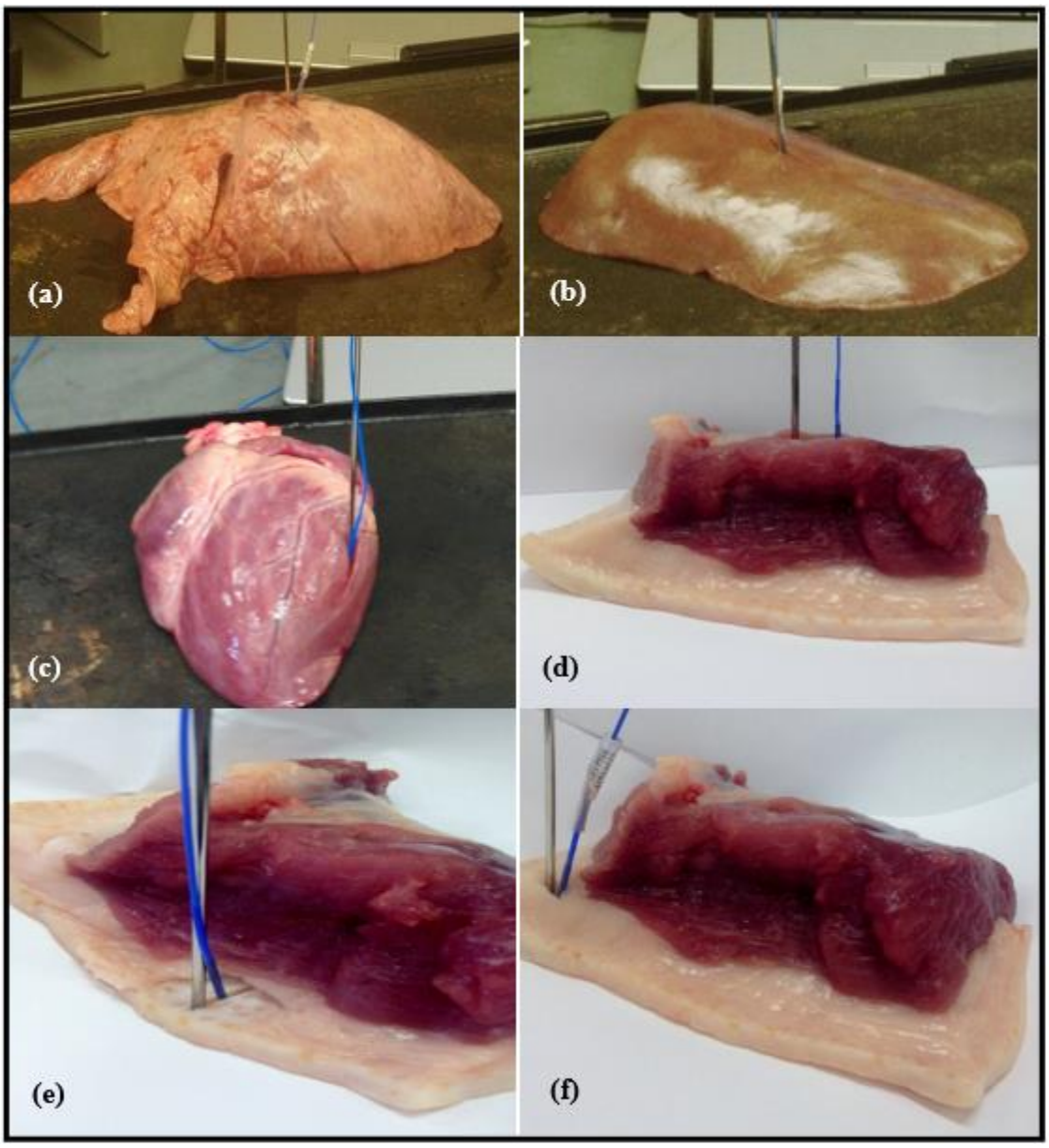

Figure 2.4 Testing Dielectric Properties of Porcine Tissue

(a) Lung, (b) Liver, (c) Heart, (d) Muscle, (e) Skin, and (f) Fat

Comparative results of the testing are shown in Figures 2.5 and 2.6. These results explain the behavior of the dielectric properties over the frequency range of 500 MHz to 10 GHz. As expected, these results act similar to those found in the Gabriel et al.

comparative data that is used in many studies as reference data for dielectric properties [8].

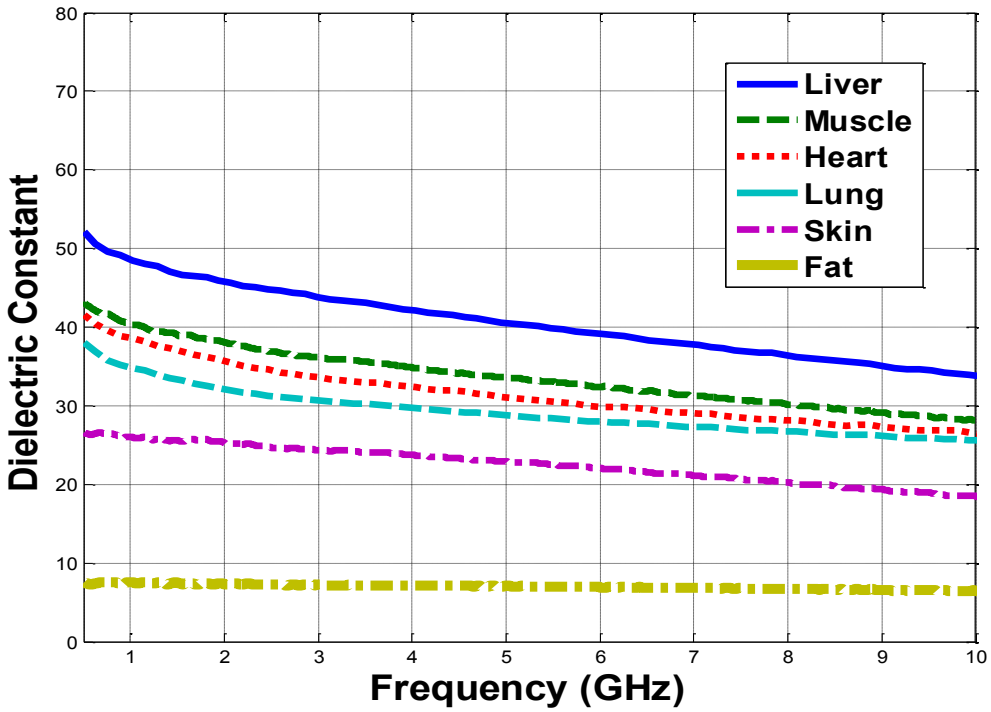

Figure 2.5 Relative Permittivity Comparison of Porcine Tissue at 25˚C

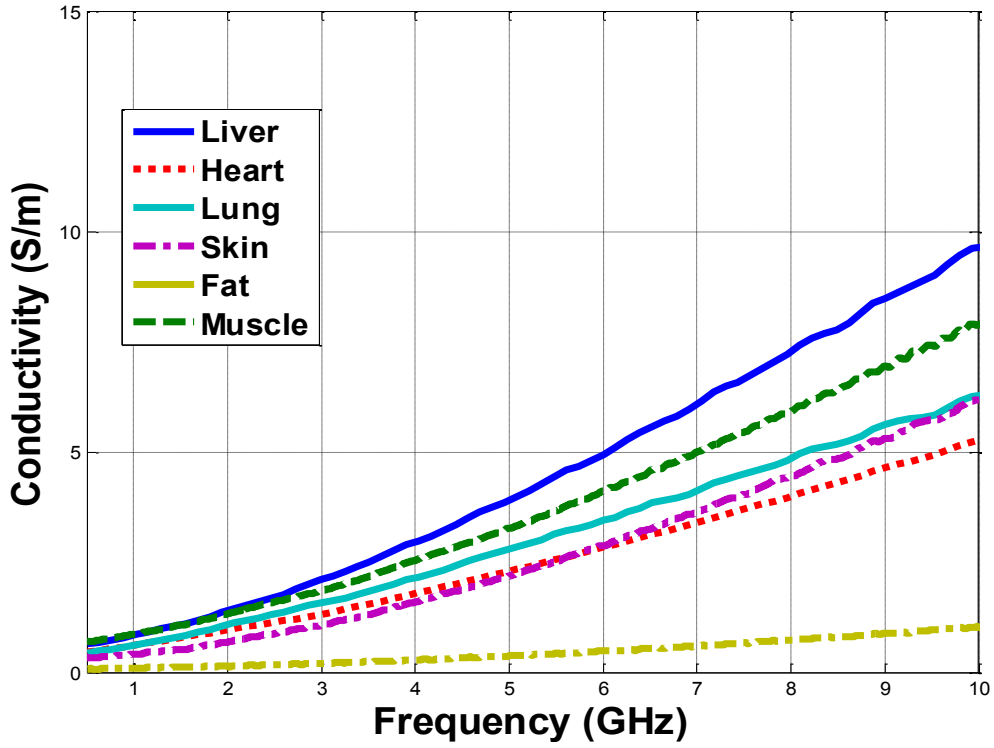

Figure 2.6 Conductivity Comparison of Porcine Tissue at 25˚C

These results display a common pattern that is related to the amount of blood found in the organs and tissues. As seen in both Figure 2.5 and 2.6, liver, which has largest percent of blood compared to the other organs and tissues, has the highest relative permittivity and conductivity. As the amount of blood found in the organ decreases, so does the relative permittivity and conductivity.

CHAPTER III

EFFECT OF TEMPERATURE ON ELECTRICAL PROPERTIES

3.1 Temperature Effects on Electrical Properties

3.1.1 Temperature Dependent Properties

Biological samples of porcine lung, heart and liver were chosen because of the similarities of electrical property to human organs [17]. The fresh samples were acquired from a local slaughter house and were all tested within 3 hours of animal death in order to maintain similar properties to that of *in vivo* testing as seen in Figure 3.1. The fiber optic temperature sensor (FISO Technologies Inc, Quebec, Canada) was used to monitor change in temperature for accurate dielectric property readings. Calibrations were made, and the fiber optic temperature sensor was tested against an IKA® ETS D5 temperature sensor to provide accurate temperature measurements.

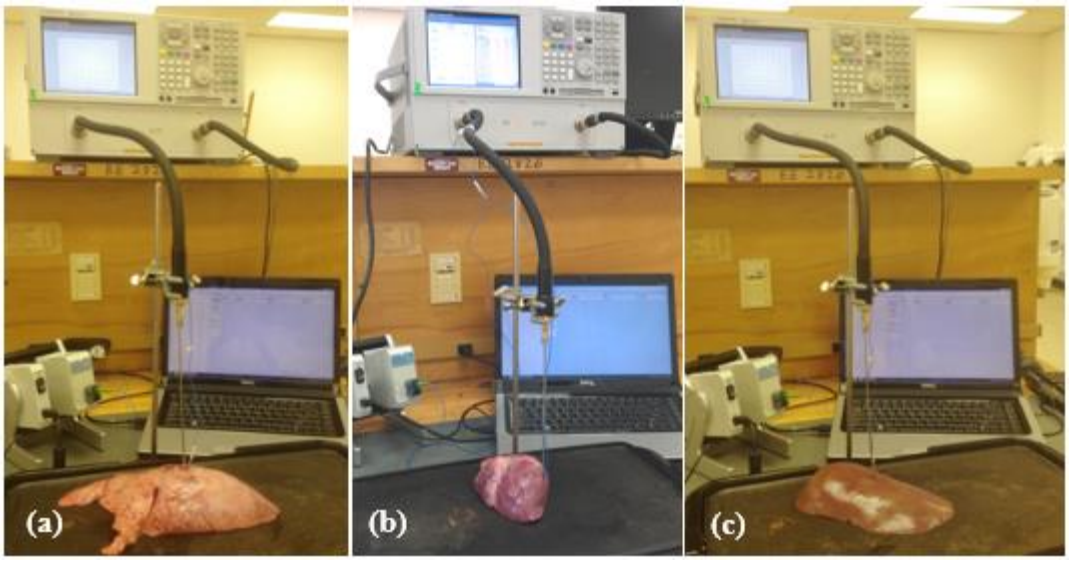

Figure 3.1 Measurement of Dielectric Properties of Porcine (a) Lung, (b) Heart, and (c) Live

Porcine samples of liver, lung and heart were then heated to temperatures of 55 to 80 degrees Celsius using a flat surface heat source. Temperatures of the ablated samples were monitored, and dielectric measurements were taken of the sample at increments of 5 degrees Celsius. The results are displayed in Figure 3.2 through Figure 3.7. It should be noted that charred regions of the samples were avoided from being tested because of a change in the tissues properties [18].

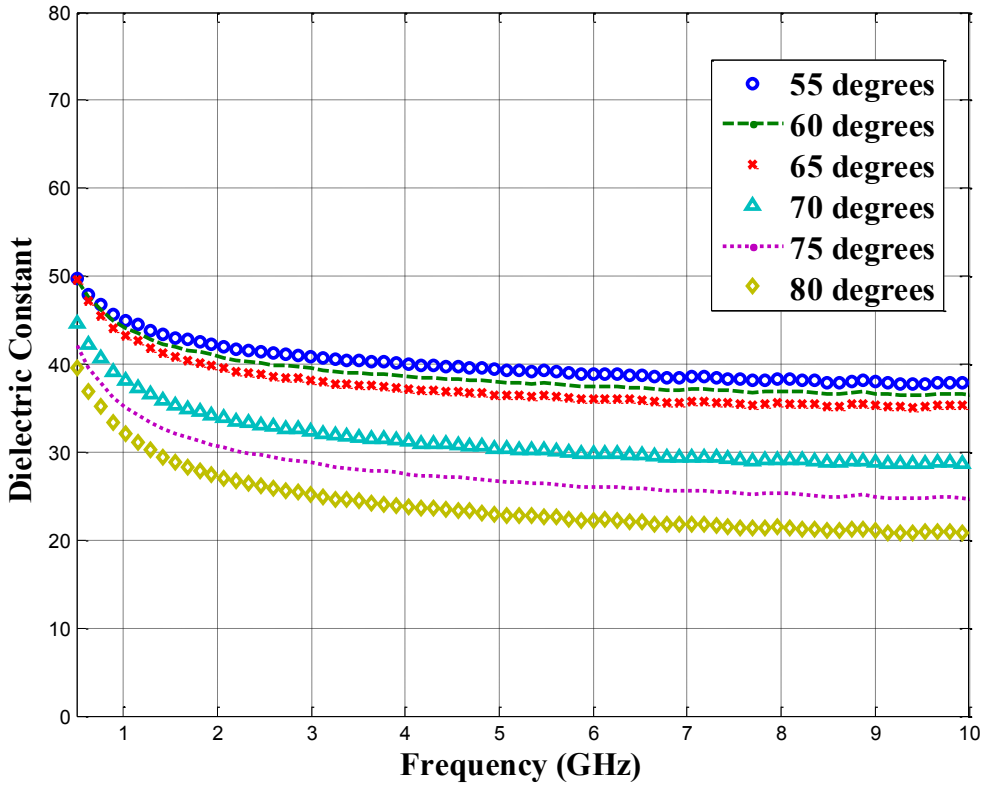

Figure 3.2 Relative Permittivity Comparison of Porcine Heart

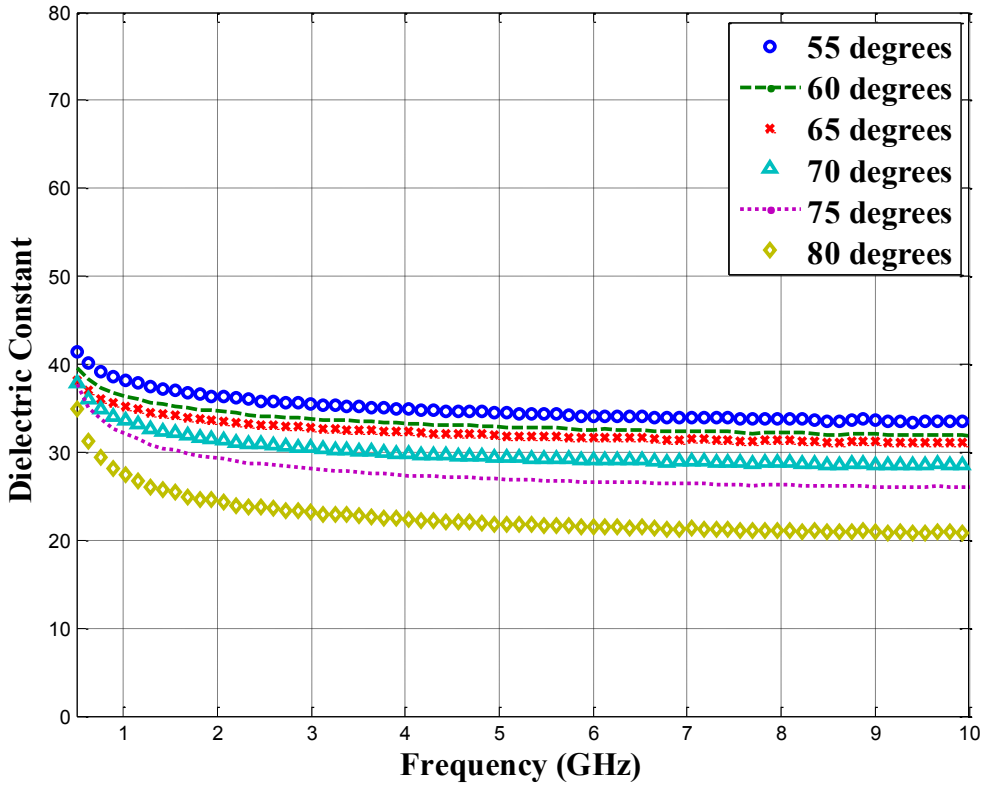

Figure 3.3 Relative Permittivity Comparison of Porcine Lung

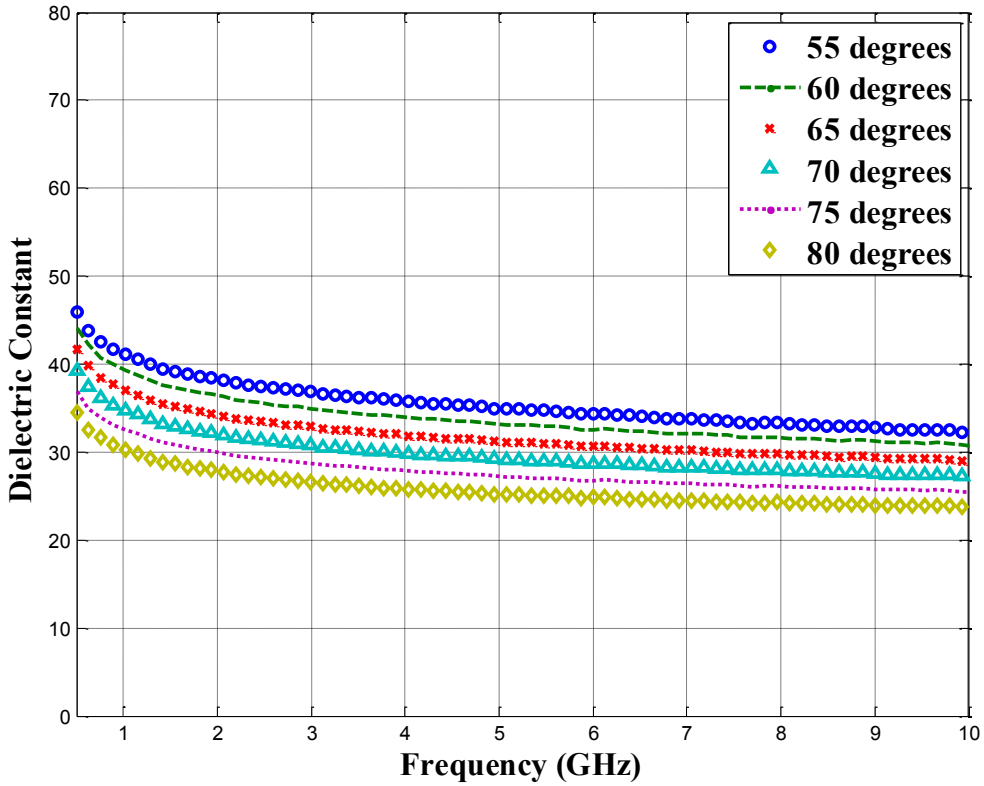

Figure 3.4 Relative Permittivity Comparison of Porcine Liver

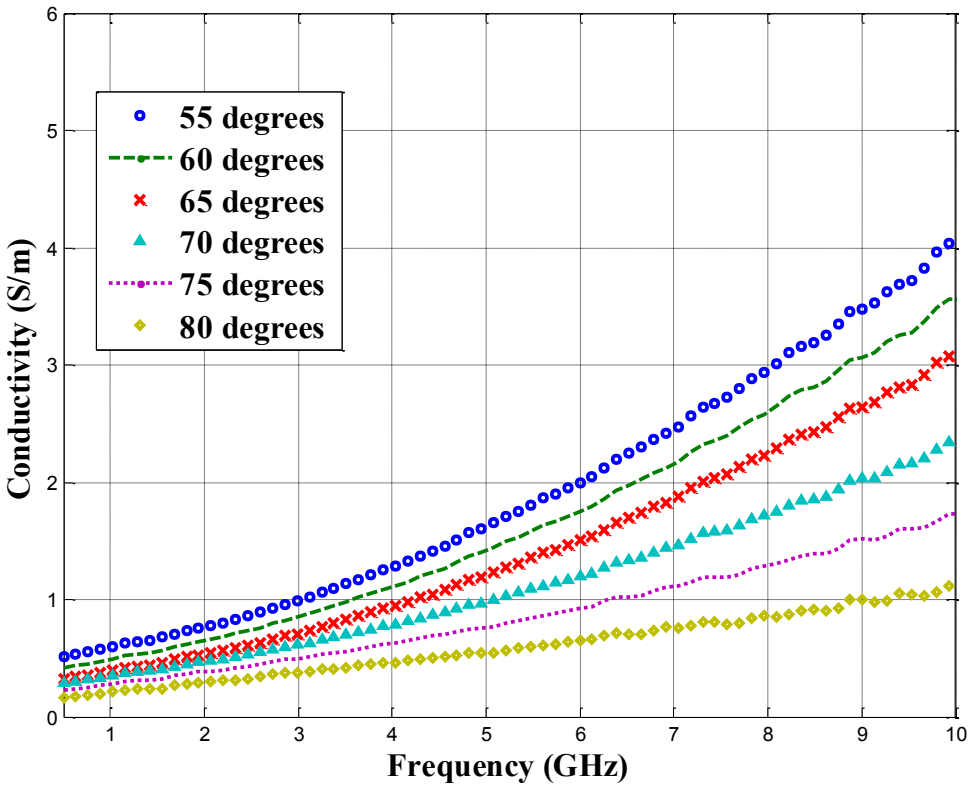

Figure 3.5 Conductivity Comparison of Porcine Lung

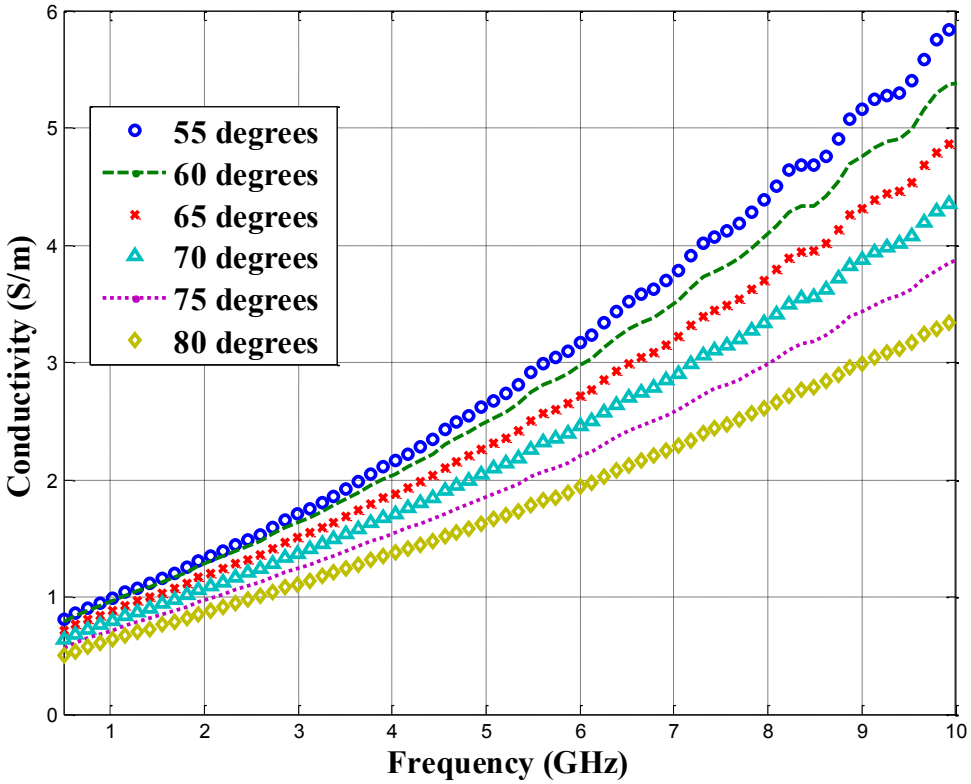

Figure 3.6 Conductivity Comparison of Porcine Liver

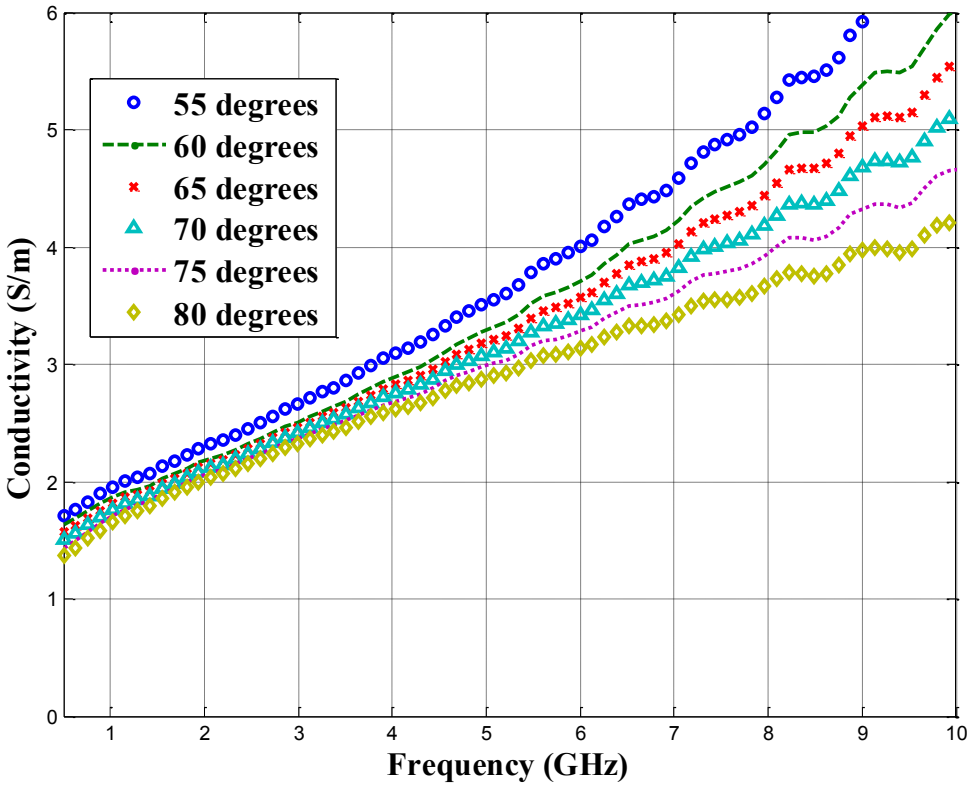

Figure 3.7 Conductivity Comparison of Porcine Heart

These results display a common pattern that is related to the amount of blood found in the tissue. As seen in Figure 3.2 through 3.7, as the temperature within the tissue increases, blood within the organ begins to either evaporate or dissipate from the location of the ablation procedure. This causes both the relative permittivity and the conductivity of the tissue to decrease as the temperatures continue to rise.

3.2 Radio Frequency and Microwave Ablation

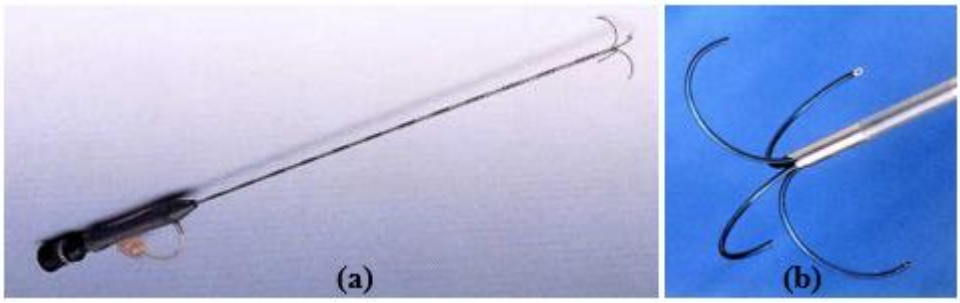

Figure 3.8 Radio Frequency (a) Applicator and (b) Thermocouple Prongs for Ablation

Radio frequency (RF) ablation has been the primary therapy of all ablation procedures for many years. It has mainly been used for the treatment of heart arrhythmias and liver tumors by increasing the temperature of the tumor tissue to around 60 ^{o}C [20]. The RF ablation generators operate at very low frequencies (mainly 480 kHz), and the power levels can be as high as 200W. This procedure requires a ground pad located in the vicinity of the RF probe to create a closed circuit between the probe and the ground. RF ablation is preferred because of ease of use and safety in surgical settings [21]. However, there are several issues associated with this procedure. It depends on the conduction of electrical energy into the tissue, so it is limited to use of one probe. As included in studies about RF ablation, the size of the targeted region of the tissue increases quickly at the beginning of the heating. Because the impedance rises, the rate of increment decays exponentially [22]. Increment in impedance makes water vaporization act as an electrical insulator which is one of the limitations for RF ablation [23]. When the tissue heats up, the tissue conductivity significantly drops and creates an open circuit limiting the ablation zone diameter. Therefore, the ablation zones are small (mm range),

and ablation times are extended (more than 10 minutes). In addition, the ground pads can cause skin burns, and because of the small ablation zones, RF is often inadequate to treat many tumors using single probes [24-26].

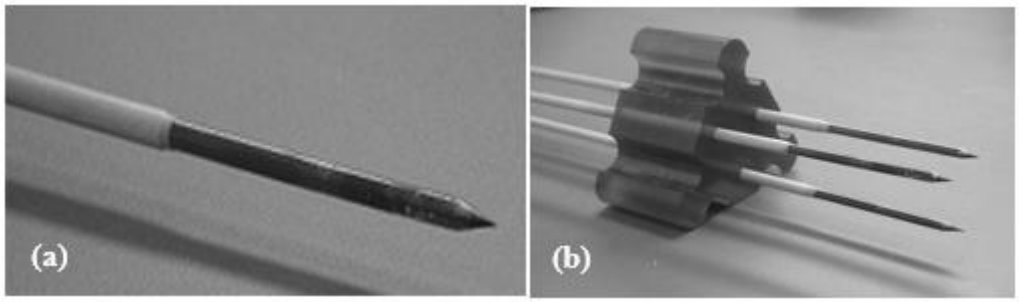

Figure 3.9 Microwave Ablation Applicator
(a) Single Probe and (b) Multiple Probes [27]

Microwave ablation (MA), since its design does not require harmful chemicals or grounding plates, gives a more flexible treatment plan and is more accommodating than most other ablation techniques because of its simplicity. It also allows for faster ablation times and larger tumor ablation volumes because of the process. MW ablation allows for single or multiple probed applicators as seen in Figure 3.10. Depending on the size or shape of the tumor, the number of probes is chosen [27].

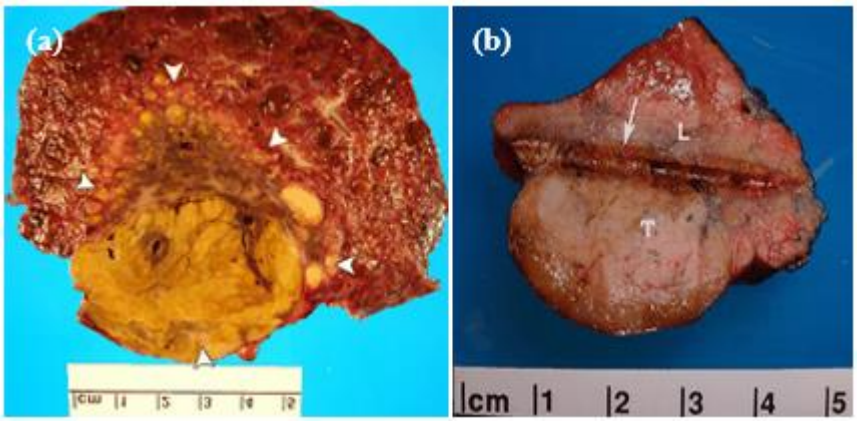

Figure 3.10 MW Ablation Zones

(a) Multiple Probes Applicator and (b) Single Probe Applicator

MA is a form of electromagnetic therapy that when focused on cancerous or tumor cells within the body, the electromagnetic waves stimulate necrosis of the cell through disruption of the water molecules. A large amount of heat is produced from electromagnetic waves that pulse through an antenna which is placed on the region of concern. Production of friction and heat from this agitation causes cellular death thus eliminating the need for more invasive surgery [28]. In order for optimum results of MA to be reached, in depth research of the dielectric properties must be done on the biological tissue of interest. This includes exploring the impact of thermal absorption during MA. It is commonly understood that negative results occur from radiofrequency and microwave ablation therapies because of the "heat sink" effect. There are many parameters that influence the "heat sink" which can be dependent on the amount of blood in and around the tumor. Results also may vary from previous studies focusing on non-human test subjects [29]. Most knowledge of this effect is unknown, but, it is possible that the deep penetration of MA can overcome the displaced heat loss, resulting in more effective

necrosis of perivascular tissue in the liver, especially with optimal dielectric tuning of the MA system to the target tissue [30]. Because most MA functions on a narrowband wavelength, power transmission efficiency is degraded once temperature changes, as seen in Figure3.11 [31].

Time (min)	MW power	Temperature (°C)		Relative permittivity (ε_r)		Conductivity (σ, S m^{-1})	
		Mean	U(95%)	Mean	U(95%)	Mean	U(95%)
0	ON	15.0	4.46%	44.98	2.01%	1.79	5.18%
1	ON	48.1	3.57%	43.43	3.36%	1.71	6.14%
2	ON	74.7	4.99%	40.65	6.46%	1.66	6.22%
3	ON	82.3	4.01%	39.22	5.76%	1.63	5.65%
4	ON	89.7	2.64%	37.66	6.42%	1.59	5.69%
5	ON	93.3	2.14%	35.26	6.07%	1.55	5.79%
6	ON	95.4	1.92%	32.12	6.58%	1.43	6.05%
7	ON	96.8	1.18%	30.47	7.19%	1.38	6.46%
8	ON	97.8	0.82%	29.04	7.49%	1.34	7.17%
9	ON	98.2	0.72%	27.61	6.58%	1.30	6.37%
10	ON	98.9	0.56%	26.76	7.13%	1.26	7.86%
12	OFF	75.2	2.43%	26.11	7.13%	1.20	8.25%
14	OFF	55.8	6.53%	26.50	7.08%	1.19	8.53%
16	OFF	48.6	6.53%	27.00	7.13%	1.19	8.54%
18	OFF	43.2	6.51%	27.60	7.19%	1.19	8.55%
20	OFF	39.6	6.56%	28.00	7.46%	1.20	9.02%

Figure 3.11 The Effect of Temperature on Porcine Liver Electrical Properties [31]

These changes in temperature alter the matching of the antenna impedance to the surrounding tissue impedance, resulting in a significant drop in power transmission efficiency. Figure 3.12 shows a dipole antenna matched to surrounding liver tissue, emulating similar dielectric properties. At 15 degrees Celsius it provides 97.5% power transmission. Temperature is increased to 98.9 degrees Celsius, and power transmission decreases to 20%.

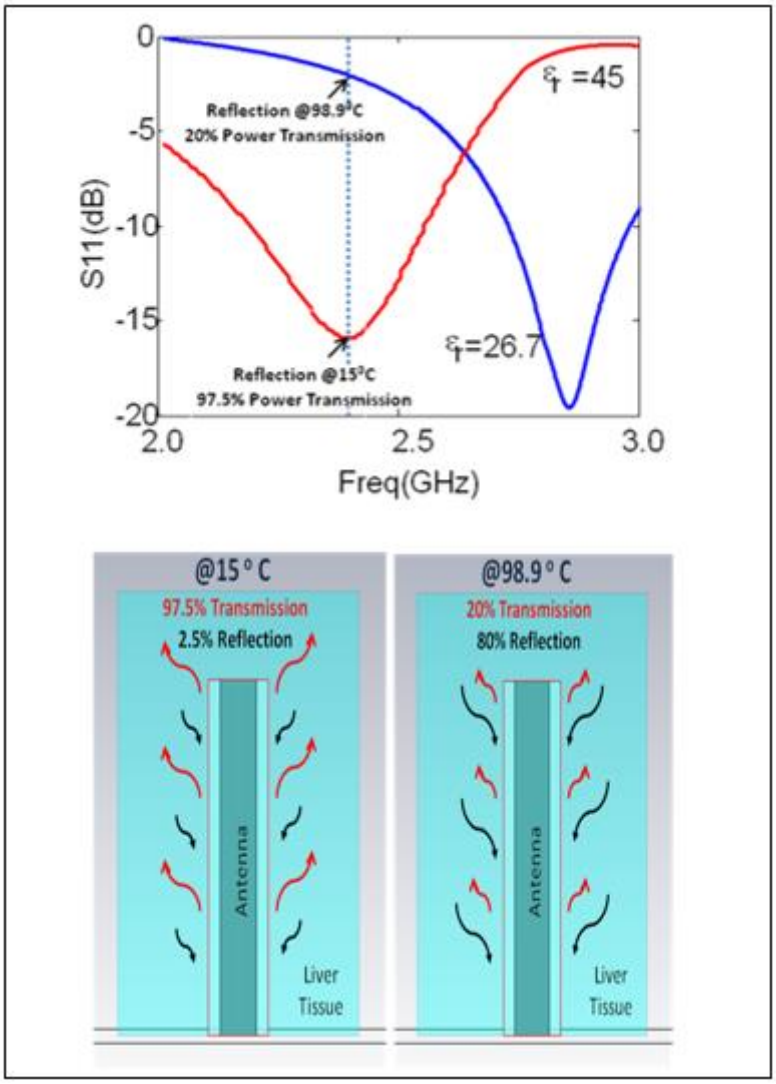

Figure 3.12 Reduction of Power Transmission Because of Changing Temperatures

In order to better understand these changes, the dielectric properties have been tested within the temperature range of 55 degrees Celsius to 80 degrees Celsius, the targeted temperature range for this study. This is required to determine specific properties necessary for proper use of the microwave ablation antenna.

The dielectric properties determine how the electromagnetic field that will be created from the MA will interact and disperse within biological tissue [32]. The results

from testing the dielectric properties of ablated tissues from porcine liver, lung, and heart will occur at a multi-frequency range from 0.5-10 GHz. Previous experimentation has been done on sealed, closed system samples from *ex vivo* bovine liver at the frequency of 915MHz [33], and *ex vivo* bovine liver at 2.45GHz [34]. Recently, research and experimentation has been documented for an open system, open sample *ex vivo* bovine liver at 2.45 GHz [35]. However, it is necessary to understand how the biological tissue reacts at multi-frequency ranges in order to increase matching of the wideband antenna to the tissue. Once this has been documented, research can continue to design a form of MA that allows for multi-frequency zones. Currently, any MA technique is done at a single frequency thus limiting the ability to vary the thermal ablation zone.

3.3 Hyperthermia

Conventional treatments for cancer are chemotherapy, radiotherapy, and surgery. Hyperthermia, (thermotherapy) can be used as an adjunctive therapy to target and raise the temperature in cancerous cells without significantly damaging normal, healthy cells. Hyperthermia has been defined as temperatures escalating in humans to above 41 degrees Celcius. At this temperature, benign tissue can tolerate extended exposure to heat, but in tumors, vascularization and blood flow are lower than that of regular tissue. This causes the cancer tissue to be more responsive to heat [36-42].

Standard tumor growth occurs at the margin and tends to extend outwardly as cells begin to mulitply. While the innermost region of a tumor characteristically has poor oxygenation and a decreased metabolism, the outer boundary maintains good nutrition and rapid heat transfer. In fact, the outermost regions of a tumor have been described to have high oxygenation and increased nutrition. This allows cancer cells to escape from

normal growth controls, but it also allows the cells to be more easily damaged from exterior influences, hyperthermia being one [42].

This form of therapy, paired with conventional therapies provides more success during cancer treatment beacuse of the exposure of electromagnetic energy as heat to the cancer cells thus reducing the resistance of the cancer treatment for the affected tissue as seen in Figure 3.13 [36-44].

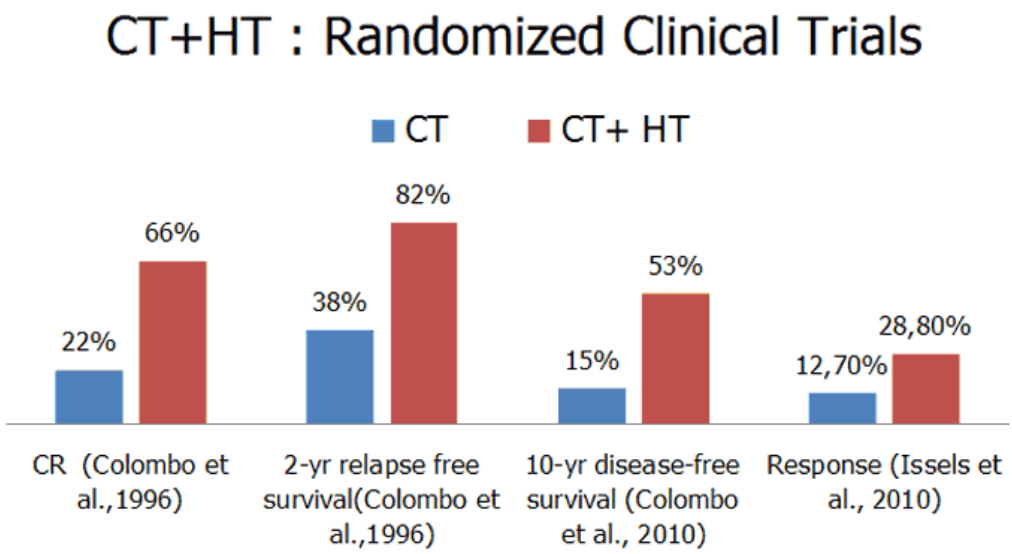

Figure 3.13 Chemotherapy Trail Results vs. Chemotherapy and Hyperthermia Trial Results

Hyperthermia causes an increase in permeablitiy of the membranes which increases the drug delivery and the radiotherapy efficiacy [38]. This property of tumors makes classical treatment more efficient when it is combined with microwave hyperthermia. Combining radiotherapy or chemotherapy and hyperthermia treatments

provides higher survial and remission rates, and it increases complete response of radiotherapy as seen in Figure 3.14 [41].

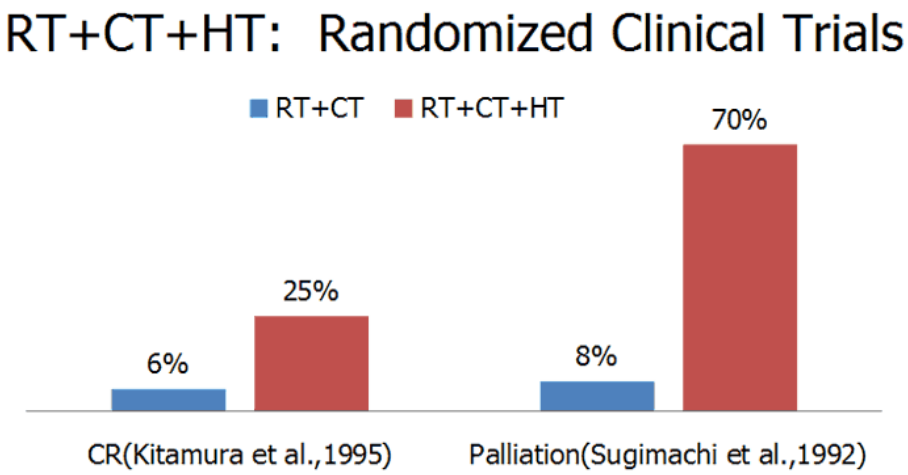

Figure 3.14 Trial Results of Carcinoma of the Rectum and Esophagial Cancer [45-46]

From this trial, a comparison was made of patients undergoing the triple modality of radiochemotherapy and hyperthermia to those patients only recieving surgery. Patients were either diagnosed with advanced carcinoma of the rectum or advanced esophagus cancer. While the most beneficial effects were seen in those patients presenting in the advanced stages of these diseases, results prove a significant difference in the five year survival rate which showed to be 91.3% survival with the triple modality versus 64% with surgery alone [47].

3.4 Antenna Applicators for MW Ablation and Hyperthermia

3.4.1 Microwave Ablation Applicator

A slot between two different media behaves like a leaky wave antenna. For a small width of the slot w_s, (compared to the media on either side of the slot) between two

different dielectric media the asymptotic value of the complex propagation constant is given by

$$k_w = \beta + \frac{k_d^2}{2\beta\left[1 - \frac{4}{\pi}\ln(\gamma_e k_d \frac{w_s}{8})\right]} \tag{3.1}$$

where γ_e is the Euler's constant, $k_d = \sqrt{k_2^2 - k_1^2}$, $\beta = \sqrt{(k_2^2 + k_1^2)/2}$, and $k_i = k_o\sqrt{\varepsilon_{ri}}$ with i=1,2 and k_o is the free space propagation constant. The rays are launched in the dielectric with lower dielectric constant with an angle γ with respect to the slot axis given

$$\gamma = \cos^{-1}\sqrt{\frac{\varepsilon_{r1} + \varepsilon_{r2}}{2\varepsilon_{r2}}} \quad . \tag{3.2}$$

The above equation indicates that the direction of the main beam is essentially independent of frequency. This phenomenon is utilized to design extremely small antennas that can be used for in-body applications. For this, the high dielectric constant of human tissues and low permittivity and low loss material like FR4 epoxy on which the antenna is printed has been exploited. The geometry of the antenna used for ablation consists of slot which is coiled in a small area (5.5 mm x 5.5 mm) printed on FR4 substrate and microstrip line printed on the back side which provides the excitation as seen in Figure 3.15. The antenna is provided with a tapered tip FR4 substrate for ease of insertion into the tissue. The slot, when excited with a suitable microstrip excitation, generates leaky waves over a very large bandwidth. Because the resulting antenna is ultra-wideband in nature, the power transmission efficiency is between 95% and 99.9% for all frequencies from 300 MHz to 10 GHz in liver as seen in Figure 3.16.

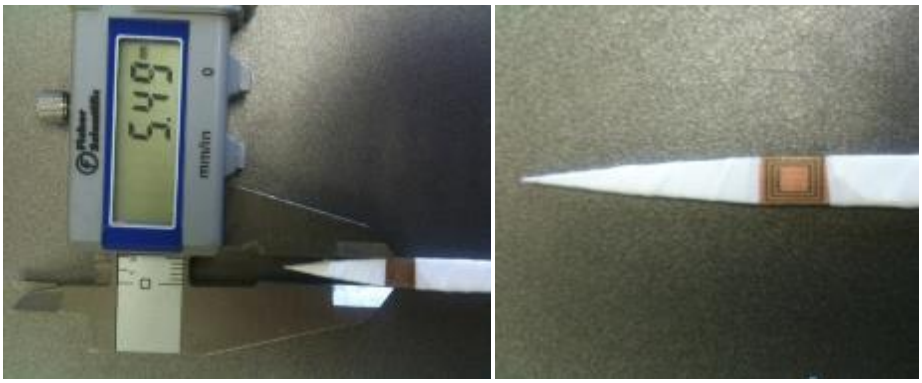

Figure 3.15 Geometry and Dimension of the Antenna (Ultra-Wideband Probe) Used for Ablation

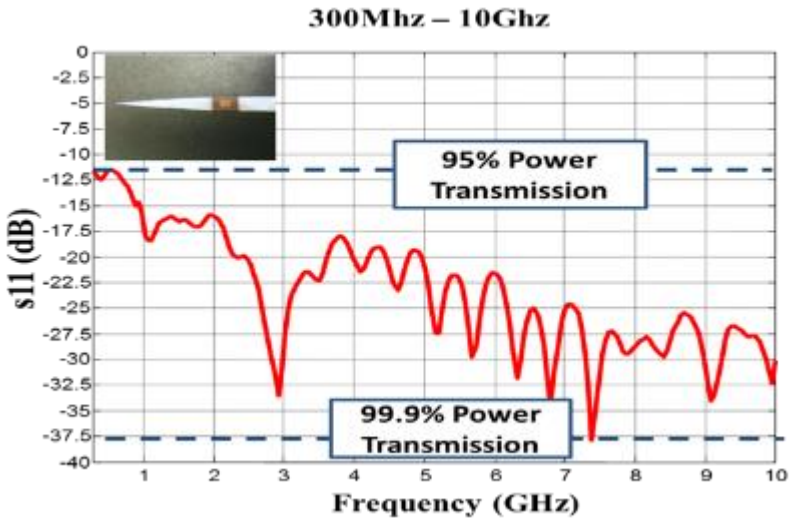

Figure 3.16 Antenna Reflection from 300 MHz - 10GHz

The top, bottom, and side views and the radiating antenna design and fabricated probe are shown in Figure 3.17 (a) and (b), respectively. The initial measurements and simulation are performed by using dielectric properties of skin, and Figure 3.18 shows the comparison of return losses simulated and measured in skin-mimicking gels. It has an ultra-wideband characteristic, meets the desired band (ISM band) and works better in

measurements. Dimensions of the probe are seen in Table 3.1. In addition, specific absorption rate (SAR) shown in Figure 3.19 is simulated in HFSS to see the effect of the antenna conformed on a 13 gauge probe on human tissue.

Currently, the antennas are printed on plane substrate for the sake of simplicity; however, in the final prototype, the purpose is to modify the antennas to conform on a 13 to 17 gauge probes.

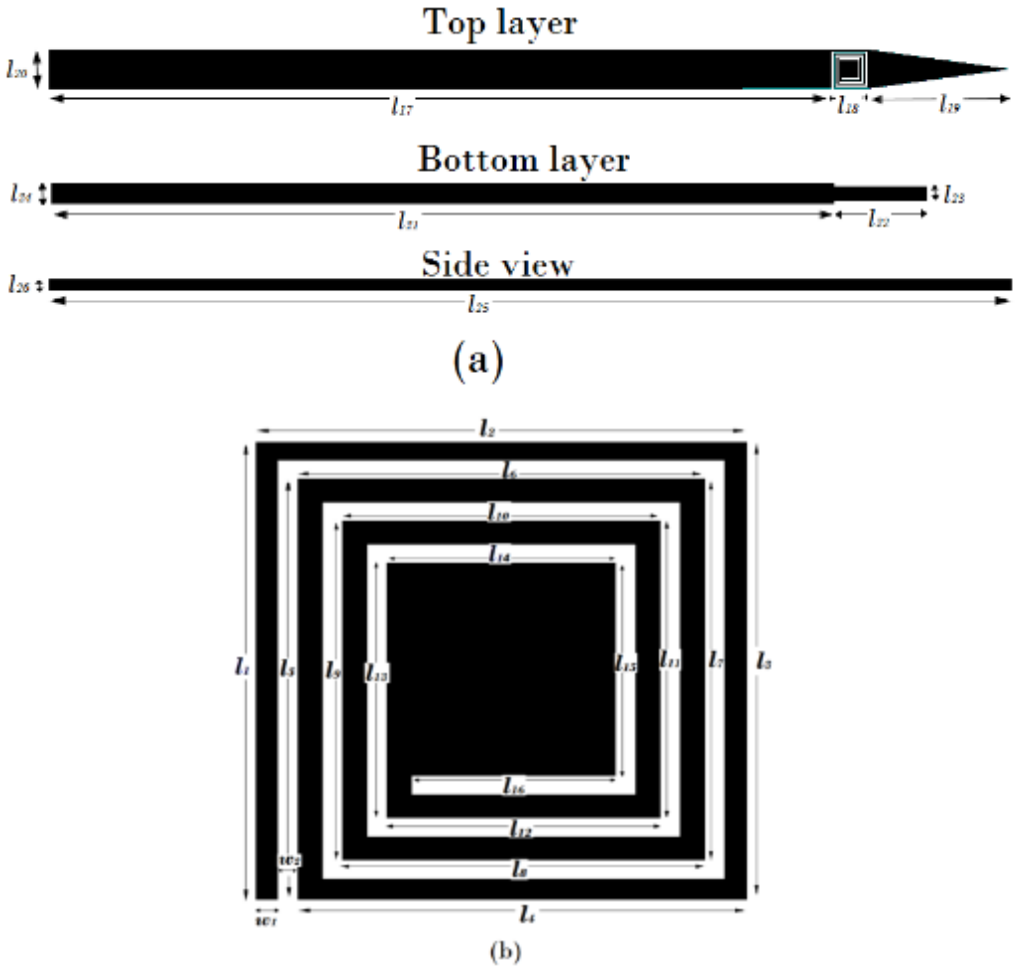

Figure 3.17 (a) Ablation Probe Used in Liver Test and (b) Radiating Antenna of the Probe

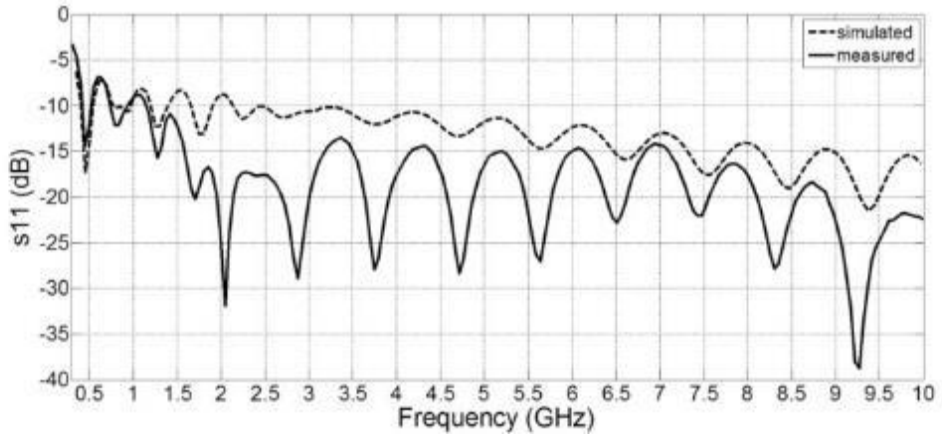

Figure 3.18 Simulated (Doted) and Measured (Solid) Return Losses

Table 3.1 Dimensions of Probe

Symbol	Dim.(mm)	Symbol	Dim.(mm)
l_1	5,5	l_{15}	2,5
l_2	5,5	l_{16}	2,25
l_3	5,5	l_{17}	150,25
l_4	5	l_{18}	5,25
l_5	5	l_{19}	20
l_6	4,5	l_{20}	5,5
l_7	4,5	l_{21}	150
l_8	4	l_{22}	15,5
l_9	4	l_{23}	2
l_{10}	3,5	l_{24}	3
l_{11}	3,5	l_{25}	157,5
l_{12}	3	l_{26}	1,5
l_{13}	3	w_1	0,25
l_{14}	2,5	w_2	0,25

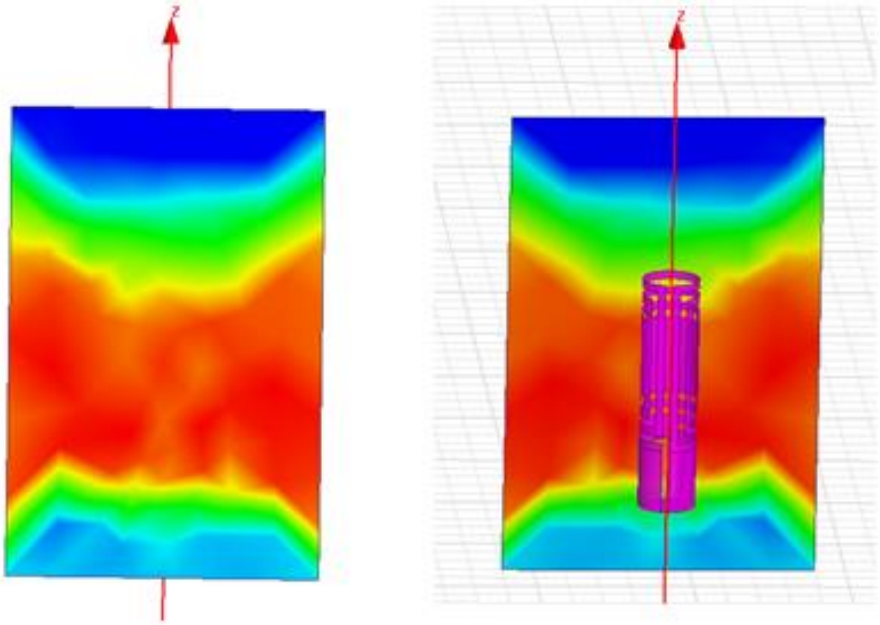

Figure 3.19 Specific Absorption Rate (SAR) of Antenna

In this study, the focus is 915 MHz, 2.4 GHz and 5.8 GHz included in ISM band (Industrial, Scientific, and Medical Band). The experiment setup which includes signal generator, amplifier, ablation probes, fiber optic temperature sensors, porcine liver and network analyzer is shown in Figure 3.20. After the probe placed into the liver, signal has been amplified up to 20W and pumped through the probe. During this experiment, temperature is observed by the sensors. In Figure 3.21, preliminary results are shown from *ex-vivo* porcine liver experiments. These measurements prove that ultra-wideband MA eliminates the unwanted ablation regions and allows adjustable ablation zones as seen Figure 3.21(b) and 3.21(c) by changing the input frequency. In addition, the power levels and ablation times are significantly lower than previously reported in the literature. The results in Figure 3.21 were generated using 20W input power with only 4 minutes of ablation. Also note that in Figure 3.21, presented is the first ever MW ablation at 5.8 GHz

which is more circular and smaller than the zone at 2.4 GHz. It is envisioned that higher frequencies (5.8 GHz or higher) can be used for small tumors that require smaller zones while lower frequencies (2.4 GHz, 915 MHz or lower) can be used for larger tumors.

Figure 3.20 Measurement Set-up for Testing Applicator

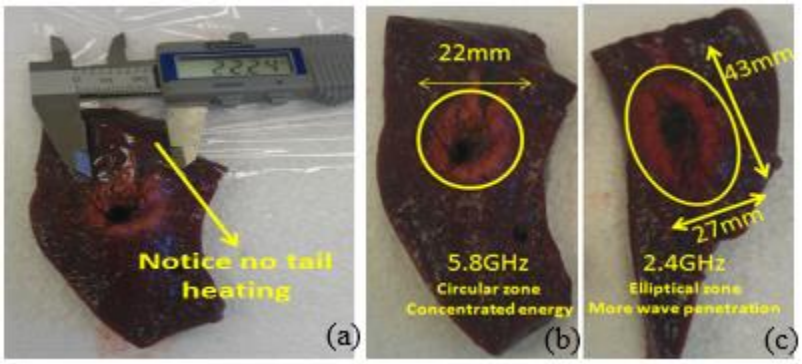

Figure 3.21 Results from MW Applicator Displaying Ablation Zones

3.4.2 Hyperthermia Applicator

In order to make it more feasible and applicable, low power and suitable applicators should be used. The goal of this research is to raise the temperature of the whole organ or tissue a few degrees, and then allow conventional therapies to destroy the cancerous tissue without damaging the healthy cells. The temperature interval for microwave hyperthermia is from 41°C to 45°C for cancer treatment [37]. In addition to its ease of use, this method is inexpensive, it requires low power, and therapy time is limited to 10 minutes to implement. For this purpose, the antennas have been fabricated onto a flexible material, so it is easy to give a form to antenna array on the bra. The antenna designed in [44] is used to create the flexible antenna applicator shown in Figure 3.22. It was designed on FR4 substrate.

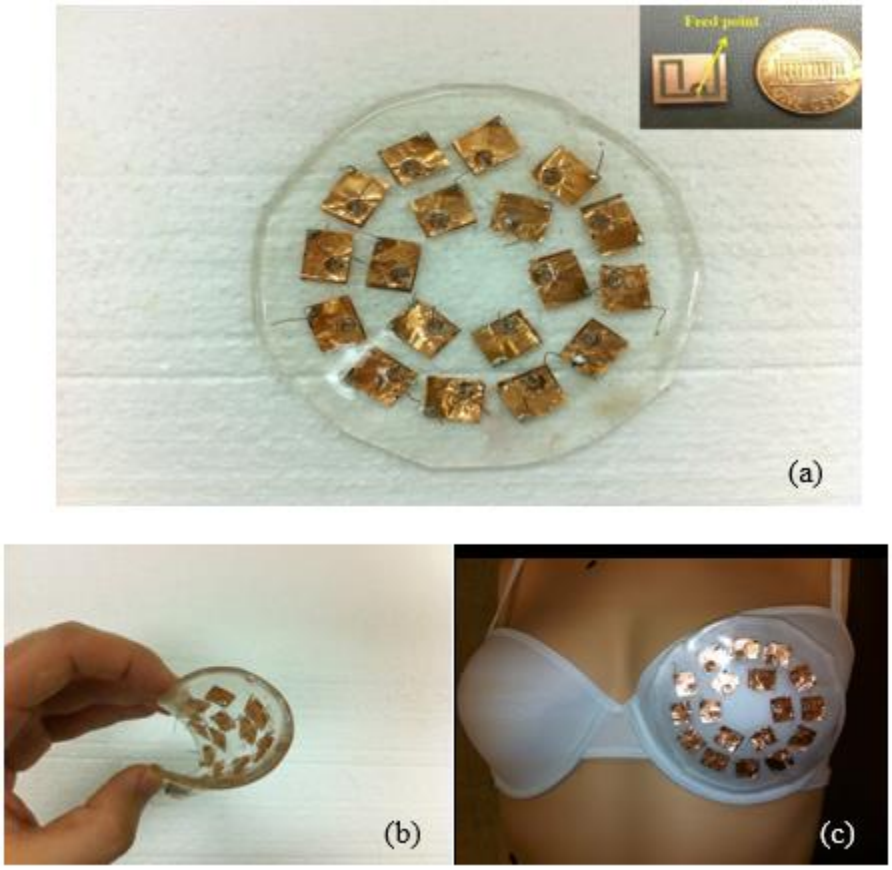

Figure 3.22 (a) Microwave Antenna Applicator (b) Printed on a Flexible Material (c) Capable of Bending to Fit the Curvature of Bra

For this application, the antenna is fabricated on a flexible material and is tested in air and on human breast-mimicking gels as seen in Figure 3.23. These gels mimick the dielectric properties of human tissue. This heterogeneous gel contains skin, fat and fibroglandular layers in anatomical likeness. It resonates at 450MHz on breast tissue well (below -10dB) but does not in air. Figure 3.24 shows the test bench including signal generator, amplifier, temperature sensors and the computer used to observe the temperature changes during testing.

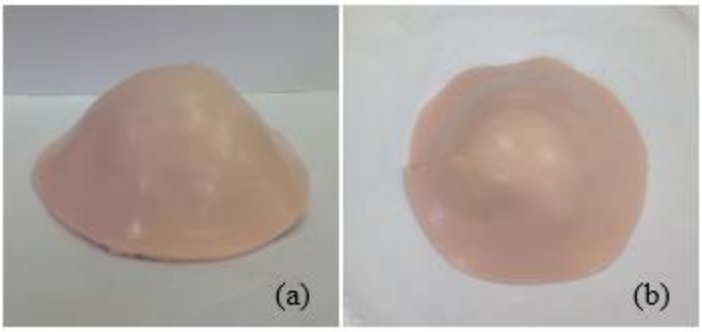

Figure 3.23 Heterogeneous Tissue Mimicking Gels of Breast

(a) Side View and (b) Top View

The microwave antenna applicator is attached on the breast-mimicking gels, and the power is pumped through the antenna as seen in Figure 3.24. Firstly, measurements were taken of the temperature rise at the depth of 1 cm with 1W power at 450 Mhz. Then, gradually increased power up to 5W and applied at 1cm depth. Thereafter, the depth was increased and repeated the measurements at 2.5cm and 4cm depths for all power levels again.

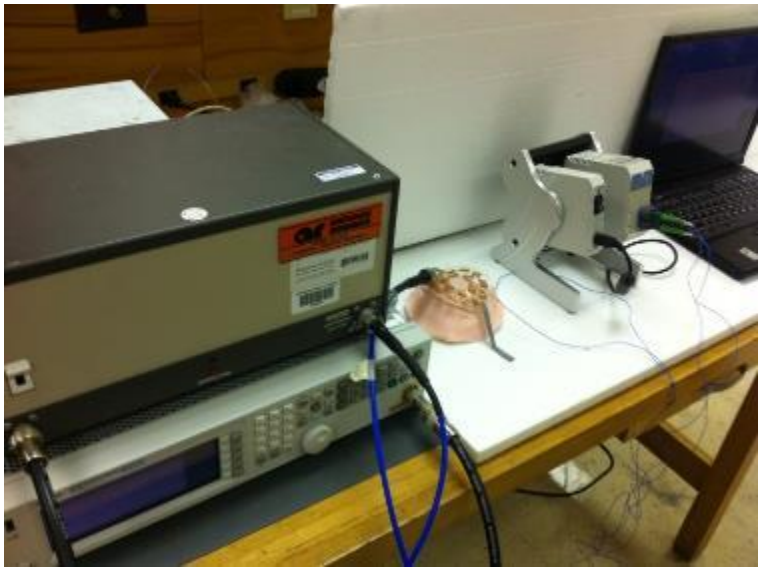

Figure 3.24 Measurement Set-up Testing the Applicator on Breast Gel

The results from the measurements in the depth of 1cm is shown in Figure 3.25. Temperature was observed in increments of 3°C at the depth of 1cm without time constraints. However, at 2.5cm and 4 cm depths, time was limited to 10, minutes and the increments were observed in temperature at the end of this period. Results for a depth of 2.5 cm are shown in Figure 3.26, and results for a depth of 4 cm are shown in Figure 3.27, respectively. Results for temperature change on the surface of the gel can be seen in Figure 3.28. Table 3.2 indicates the temperature increments, duration of applied power and duration of cooling for each levels.

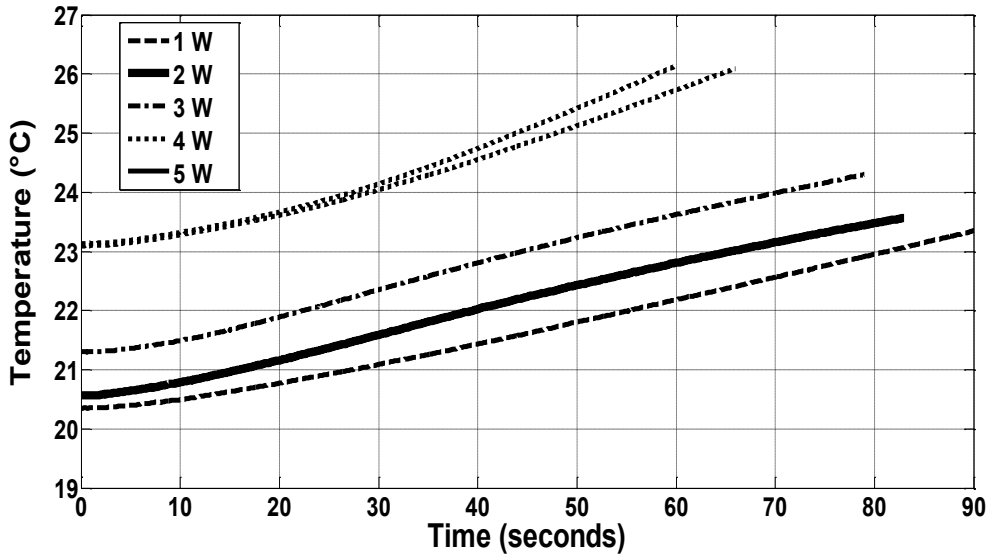

Figure 3.25 Results for Temperature Increment at the Depth of 1cm

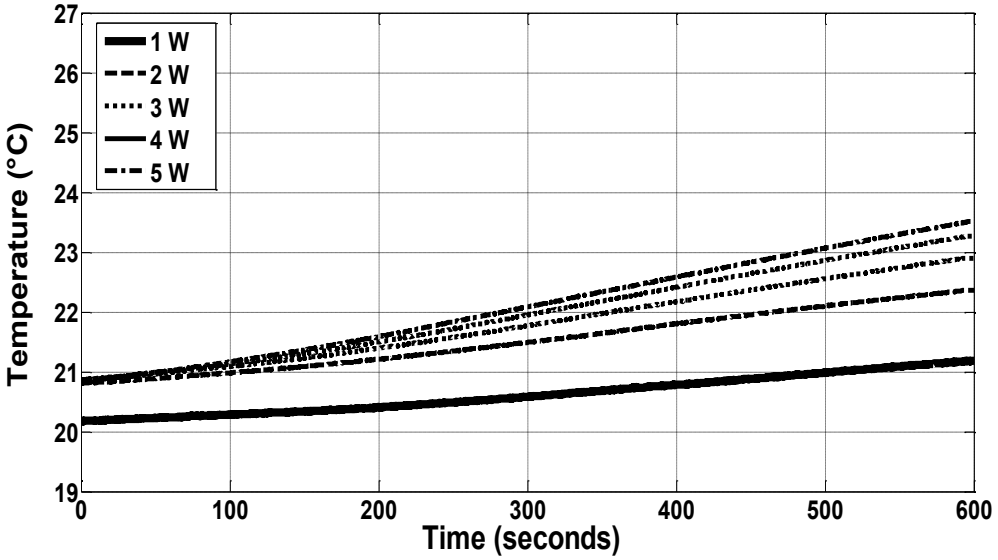

Figure 3.26 Results for Temperature Increment at the Depth of 2.5cm

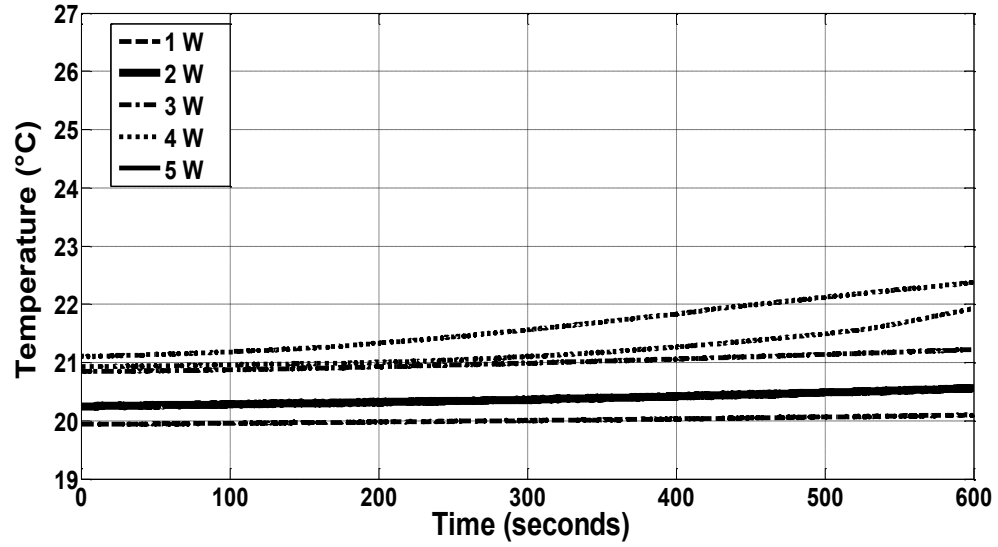

Figure 3.27 Results for Temperature Increment at the Depth of 4 cm

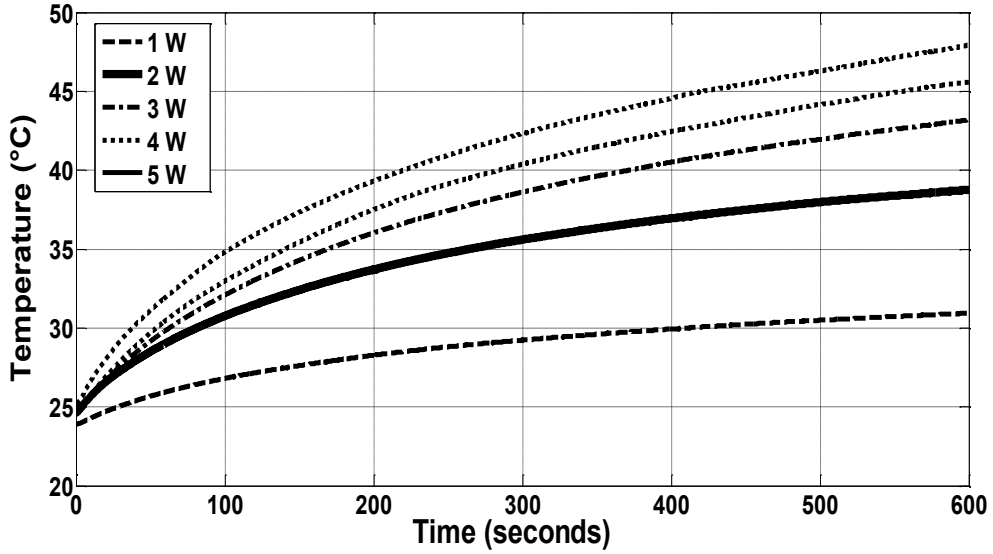

Figure 3.28 Results for Increased Temperature on the Surface of the Gel (for Each Power Level in 10 Minutes)

Table 3.2 List of Duration of Application and Cooling

	1 cm	2.5 cm	4 cm
1W	90 sec / 19 min / 3°C	10 min / 30 min / 1°C	10 min / 25 min / 0.15°C
2W	83 sec / 19 min / 3°C	10 min / 34 min / 1.55°C	10 min / 32 min / 0.313°C
3W	79 sec / 19 min / 3°C	10 min / 49 min / 2.025°C	10 min / 37 min / 0.385°C
4W	66 sec / 19 min / 3°C	10 min / 63 min / 2.4°C	10 min / 48 min / 1°C
5W	60 sec / 19 min / 3°C	10 min / 67 min / 2.644°C	10 min / 60 min / 1.28°C
	duratin of application / cooling time / increment in celcius degree		

CHAPTER IV

ELECTRICAL PROPERTIES OF BROWN ADIPOSE TISSUE AND ITS ROLE IN METABOLIC FUNCTIONS

4.1 Dielectric Properties of Brown Adipose Tissue

Adipose tissues play a critical role in the energy homeostasis of mammalian bodies. These tissues are mainly composed of white and brown adipocytes, which present different morphology and homeostatic functions [48]. White adipocytes are filled with one large vacuole of lipid that pushes the nuclei to the side of the cell (**Error! Reference source not found.**a); its main function is energy storage, in the form of triglycerides, during meals and energy release, in the form of fatty acids, between meals. Long term imbalance between energy intake and expenditure will lead to excess accumulation of white adipose tissue (WAT), which causes obesity. White adipocytes are also responsible for releasing hormones that tend to lower whole-body metabolism and promote insulin resistance, which aggravates obesity and contributes to the appearance of type 2 diabetes [49-50].

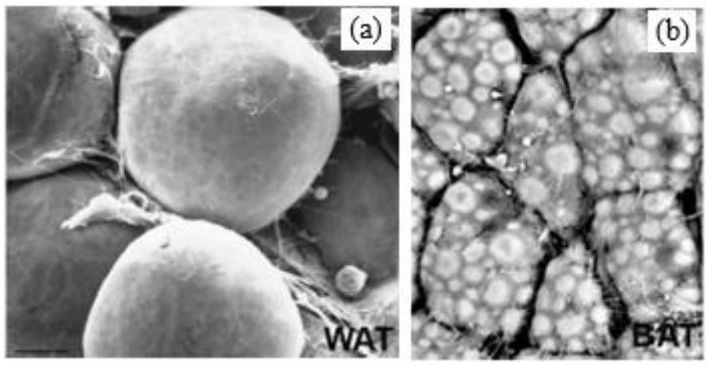

Figure 4.1 Scanning Electron Microscopy of (a) White Adipose Tissue and (b) Brown Adipose Tissue [50]

Brown adipocytes, in the other hand, present numerous smaller vacuoles in the cytoplasm (**Error! Reference source not found.**b) and are rich in large mitochondria containing the protein UCP1, uniquely expressed in these cells. UCP1 protein is responsible for uncoupling the oxidative phosphorylation that in turn is responsible for heat production [50]. This thermogenic process, that characterizes brown adipose tissue (BAT), dissipates stored energy and plays a concurrent role with WAT in the energy homeostasis. Thus, the ability to stimulate BAT activity may help mediate weight gain and insulin sensitivity [51-53].

BAT cells can be activated with cold exposure. Cold excites the sympathetic nervous system and consequent release of norepinephrine (NE) at the sympathetic nerve terminals, which profusely innervate BAT cells. This pathway leads to UCP1 activation and consequent heat generation [53-54]. The increased metabolism associated with thermogenesis is a good indicator of BAT activity; its monitorization opens new perspectives as a therapeutic target for the treatment of obesity and associated diseases such as type 2 diabetes and metabolic syndrome [49, 53, and 55].

BAT was thought to exist in significant amounts only in infants, small animals and during hibernation. Using PET/CT (positron emission tomography / computed tomography), however, metabolically active BAT was recently found in defined regions along the upper chest and upper back of adults [56-57]. PET/CT have proven most effective for locating BAT because of its high uptake of 18F-FDG [58-60]. These studies are expensive however and risks associated with radiation exposure prevent repetitive scanning. Magnetic Resonance Imaging (MRI) has also been used but is similarly expensive [61-62]. Infrared thermography is a passive approach that has demonstrated feasibility in locating BAT by detecting the increased metabolic activity from conduction of locally increased temperature at depth to the skin surface [63]. However, infrared thermal imaging is not sufficiently sensitive to quantify small changes in the metabolic activity of subsurface BAT since it is particularly affected by blood flow of underlying tissues and environmental conditions [64]. All three imaging techniques are logistically unsuited to continuously track BAT activity over a long period of time.

A new technology has to be developed to facilitate studies of BAT metabolic activity: it must be painless, non-toxic, reliable, and inexpensive enough for long term monitoring in large patient studies. Microwave radiometry was recently proposed since it fits all these requirements [65-66]. This technique is based on non-invasive collection of thermal radiation emitted by any object above zero degree Kelvin, including human tissues such as brown fat. The received power is further calibrated and converted into a volume-averaged measure of absolute temperature of the deep target [66-69]. The conversion algorithm relies on proper characterization of electromagnetic wave

propagation within the medium. In the case of human tissues, their chemical structure dictates a lossy dielectric behavior that is determined by dielectric properties [70].

Methods: Six female rats (*Rattus Norvegicus*) were obtained from the Mississippi State University College of Veterinarian Medicine. They weighted approximately 200g and were presented in good health. The most studied, typical, brown adipose deposits in rodents are located in the interscapular region [71]. After euthanasia (CO2 monitored until confirmed death), the skin was removed from the interscapular region, and BAT could be easily identified between the shoulders (Figure a). The dielectric properties were then measured using the dielectric slim form probe kit from the Agilent E85070 network analyzer as seen in Figure b.

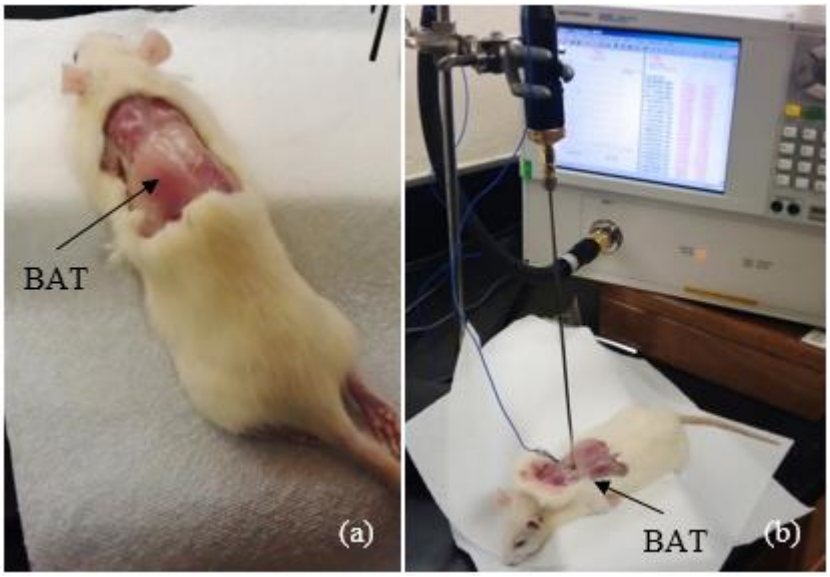

Figure 4.2 (a) Brown Adipose Tissue and (b) Measuring the Dielectric Properties while Monitoring the Internal Temperature

Since dielectric properties are temperature dependent, BAT internal temperature was continuously monitored using a fiber-optic temperature sensor (FISO, Quebec Canada). Results were taken around 37 degrees Celsius for all six rats. Once the BAT dielectric properties were determined, a few samples of WAT were tested. These samples were taken from the lower abdomen and upper thigh regions. This process was performed for all six rats.

Results taken from 0.5 GHz to 10 GHz show that both the dielectric constant, as seen in Figure 4.3, and the conductivity, as seen in Figure 4.4, of brown adipose tissue are higher than the results from the white adipose tissue. The data show similar trends between the white adipose tissue and the brown adipose tissue.

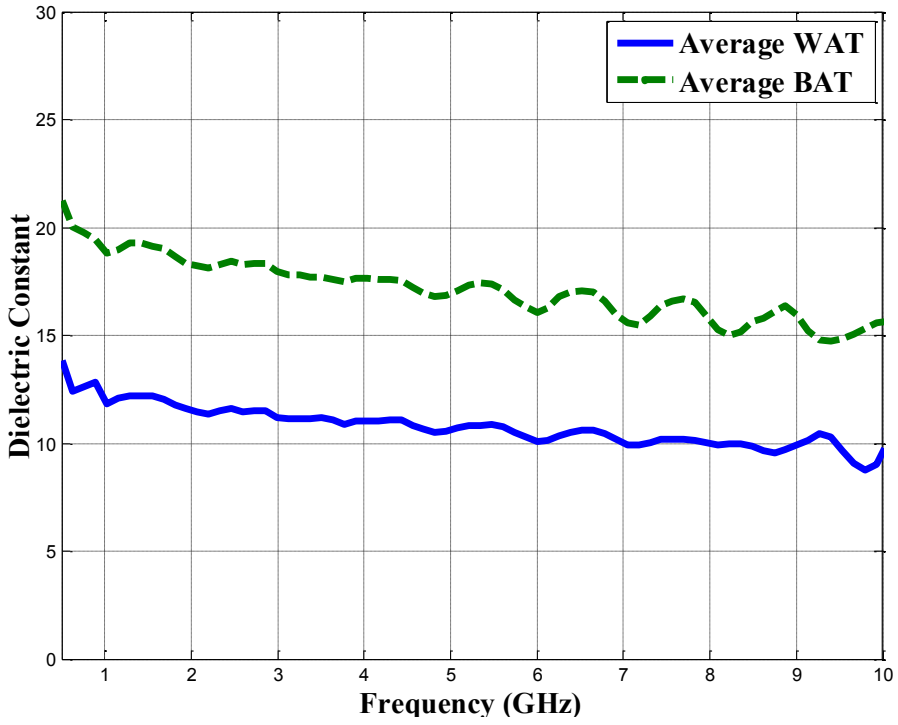

Figure 4.3 Comparison of Permittivity in White Adipose Tissue and Brown Adipose Tissue

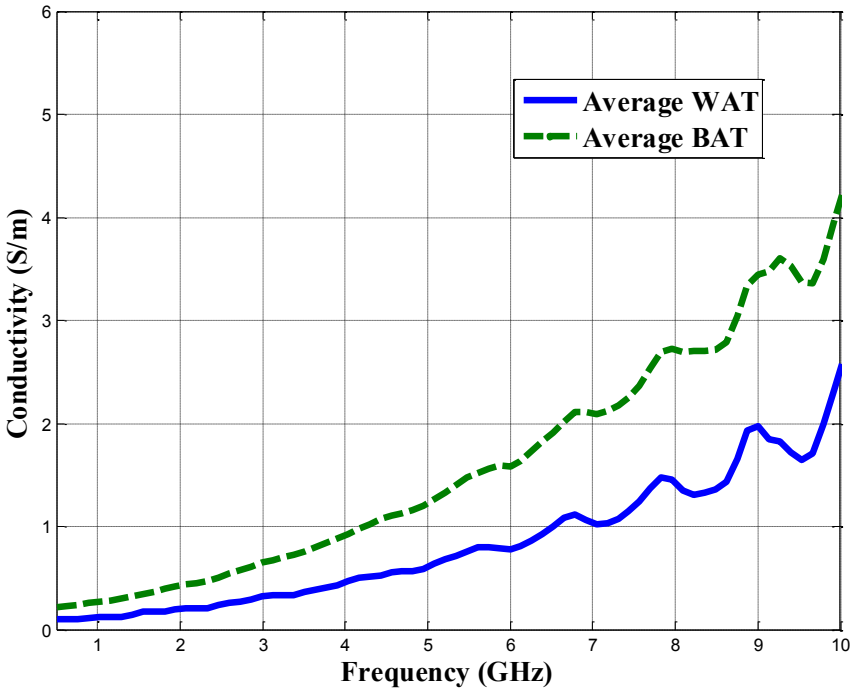

Figure 4.4 Comparison of Conductivity in White Adipose Tissue and Brown Adipose Tissue

For biological tissue, defining the interaction of electromagnetic (EM) radiation at the cellular and molecular level is necessary. Applying low frequency waves through biological tissue interferes with the ionic diffusion across cellular membranes. Introducing higher frequency waves, in the MHz region, hinders the flow of ions across membranes, mainly the flow of proteins and other organic molecules. Applying EM radiation at high frequencies, spanning into the GHz region, polarizes water molecules within the cell [8]. Polarization of water molecules causes increased viscosity within the cell. Increased viscosity along with disruption of the diffusion of molecules across permeable membranes ultimately interrupts biological and chemical processes preventing

normal activity of the cell [72]. Understanding the normal state of the dielectric properties in BAT is necessary for further research of the tissue.

4.2 Thermal Modeling

Steady-state thermal simulations were performed in COMSOL® to address two distinct scenarios: cold and noradrenergic stimulation. The mesh in the heat transfer model was refined until solutions presented energy conservation and mesh independence. The simulated temperature distribution and the electromagnetic simulations were combined using equations 4.1 and 4.2 [73],

$$P_{ant} = Gk_B T_B \Delta f \tag{4.1}$$

where (T_B) is the equivalent temperature determined from the weighted volumetric average temperature within the sense region of the antenna, (P_{ant}) is the power collected from the antenna, k_B is the Boltzmann constant and G is the radiometer global gain. For the equation,

$$T_B = \int_{\Delta f} \left(1 - |S_{11}(f)|^2\right) \left(\int_V W(\vec{r}, f) T(\vec{r}) dV + T_{EMI} \right) + |S_{11}(f)|^2 T_{REC}\, df \tag{4.2}$$

defining $T(r)$ as the physical temperature in the human tissue located at the position r within a sensing volume V, the radiometer receiver noise temperature T_{REC}, the electromagnetic interference collected by the antenna from the surrounding environment T_{EMI}, and S_{11} as the power reflection coefficient because of the mismatch at the antenna/load interface, the temperature measured by the radiometer in the band Δf is given to compute the theoretical power received by the antenna. The receiver temperature T_{REC} = 95 K was taken from literature [74]. As a result, **Error! Reference source not**

found.4.5 and **Error! Reference source not found.**4.6 show the theoretical radiometric power variation as a function of metabolism (W/m^3) for cold and noradrenergic stimulation, respectively. In either case the average simulated power is -86.7 dBm.

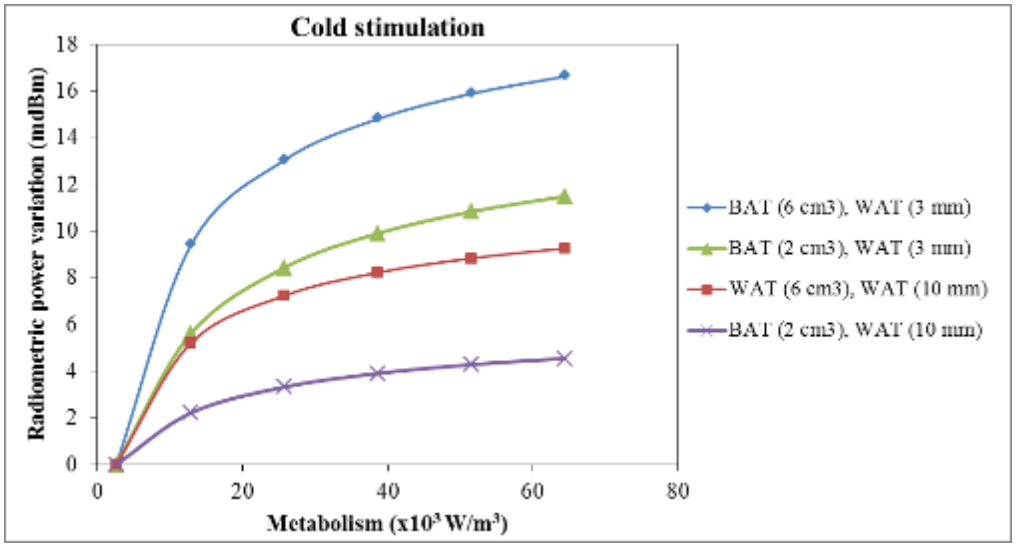

Figure 4.5 Parametric Simulations to Assess Antenna's Sensitivity to Metabolic Variations Under Mild Cold Simulation (15 °C)

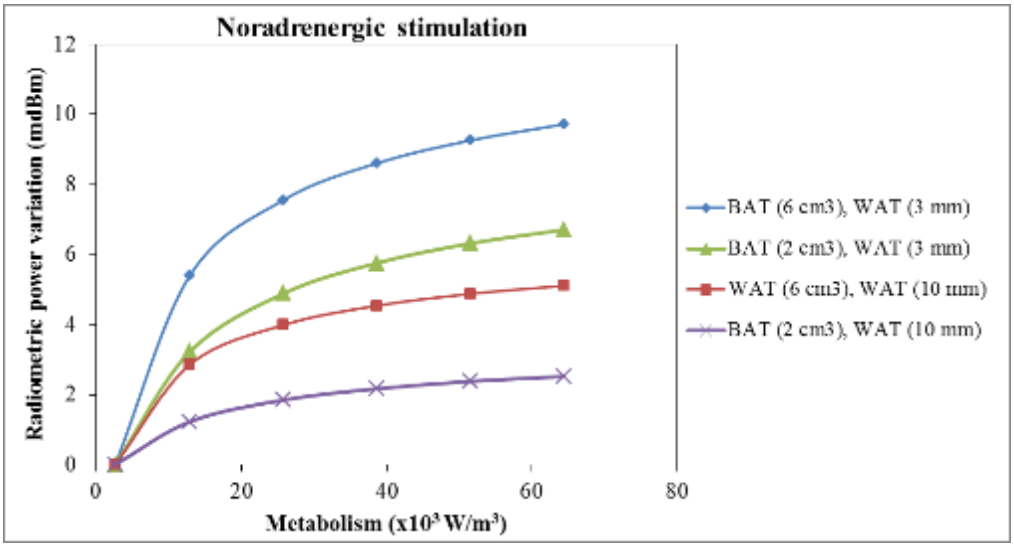

Figure 4.6 Parametric Simulations to Assess Antenna's Sensitivity to Metabolic Variations Under Noradrenergic Simulation (15°C)

Error! Reference source not found.4.1 presents descriptive data for average BAT temperature at baseline and after 15-fold increased metabolism. Both stimulation inductors are compared. Within all simulated scenarios, the antenna sensitivity was 3.9-12.2 mdBm/°C, corresponding to detection of temperature variations as small as 0.6°C at 12 mm depth.

Table 4.1 Sensitivity of Radiometric Antenna and Average BAT Temperature for All Model Configurations During Cold and Noradrenergic Stimulation

BAT volume (cm^3)	WAT thickness (mm)	Stimulation	Baseline average BAT temperature (°C)	Temperature variation for 15-fold increased metabolism (°C)	Sensitivity (mdBm/°C)
6	3	Cold	36.00	1.12	12.19
		Noradrenergic	36.58	0.70	11.34
6	10	Cold	36.34	0.89	8.60
		Noradrenergic	36.80	0.62	7.56
2	3	Cold	35.74	1.29	7.83
		Noradrenergic	36.42	0.81	7.30
2	10	Cold	36.31	0.90	4.45

		Noradrenergic	36.78	0.57	3.90

By combining electromagnetics and heat transfer analysis to simulate power emitted from activated human brown fat, and received by a radiometric antenna, a new computational model was established. The rationale is based on the principle that thermal energy radiates from living tissue with a significant amount of power in the microwave frequency band. This thermal radiation can be collected with a microwave receive antenna, amplified, filtered and quantified with a sensitive power detector. With appropriate electronics and software processing, the received power can be correlated directly with temperature of tissue located within the radiation field of the antenna. Such a measurement device is termed a microwave radiometer. The design and optimization of the radiometric antenna based on tapered log-spiral geometry is the subject of this study. Once the design is established, thermal modeling and radiometry principles will mediate the feasibility for brown fat monitoring with microwave radiometry.

CHAPTER V

CONCLUSION

The widespread advancements made in electromagnetic devices have brought the need for a more in depth understanding of the behavior of dielectric properties in biological tissues. Recognizing and understanding the pattern of these properties once they have been introduced to parameters such as heat and frequency ranges allows medical devices to be fine tuned to specific patterns to increase efficiency. The dielectric properties of various tissues have been mapped from a frequency range of 500 MHz to 10 GHz and have been defined from a temperature range of 25 to 80 ˚C. From these results, a microwave ablation applicator and a microwave hyperthermia applicator have been designed to combat tumor grown within the human body.

Thermal modeling has also been characterized for the metabolic functions of brown adipose tissue based upon the dielectric properties measured from 500 MHz to 10 GHz at 37˚C. Using a radiometer for constant, long-term monitoring, these results will be used to better understand of the role of brown adipose tissue in human metabolic behavior.

REFERENCES

[1] Salman S, Wang Z, Colebeck E, Kiourti A, Topsakal E and Volakis J 2013 Pulmonary Edema Monitoring Sensor with Integrated Body-Area Network for Remote Medical Sensing *Phys Bio Med* (Submitted)

[2] Asili M, Colebeck E, Chen P, Demirci U and Topsakal E 2013 Flexible Microwave Antenna Applicator for Chemothermotherapy of the Breast *IEEE AWPL* (Submitted)

[3] Colebeck E, Asili M, Seran S and Topsakal E 2013 Ultra-Wideband Microwave Ablation Therapy (UMAT) *IEEE Trans Microwave Theory Tech* (Submitted)

[4] Colebeck E, Rodrigues D, Hood Z, Salahi S, Maccarini P, Stauffer P and Topsakal E 2013 Microwave Measurement of Dielectric Properties of Brown and White Adipose Tissue in Rats *Phys Bio Med*

[5] Nacke T, Barthel A, Cahill B, Meister M and Zaikou Y 2013 High Frequency Fluidic and Microfluidic Sensors for Contactless Dielectric and in Vivo Cell Culture Measurement Applications *J Physics* **434** 1-4

[6] Chow E, Morris M and Irazogui P 2013 Implantable RF Medical Devices *IEEE Microwave Mag.* 64-73

[7] Miklavcic D, Pavselj N and Hart F 2006 Electrical Properties of Tissues *Wiley Encyclopedia of Biomed. Eng.* 1-12

[8] Gabriel C, Gabriel S and Corthout E 1996 The Dielectric Properties of Biological Tissues: I. Literature Survey *Phys. Med. Biol.* **41** 2231-2249

[9] Foster K and Schwan H 1989 Dielectric Properties of Tissues and Biological Materials: a Critical Review *Crit. Rev. Biomed. Eng.* **17** 25-104

[10] Pethig R 1984 Dielectric Properties of Biological Materials: Biophysical and Medical Applications *IEEE Trans. Elect. Insul.* **5** 453-474

[11] Schwan H and Foster K 1980 RF-Field Interactions with Biological Systems: Electrical Properties and Biophysical Mechanism *Proceedings of the IEEE* **68** 104-113

[12] Reilly J 1998 Applied Bioelectricity *From Electrical Stimulation to Electrophathology* New York: Springer-Verlag

[13] Pethig R 1979 *Dielectric and Electronic Properties of Biological Material* New York:Wiley

[14] Gabriel S, Lau R and Gabriel C 1996 The Dielectric Properties of Biological Tissues: III. Parametric Models for the Dielectric Spectrum of Tissues *Phys. Med. Biol.* **41** 2271-2293

[15] Hurt D 1985 Multiterm Debye dispersion relations for permittivity of muscle *IEEE Trans. Biomed. Eng.* **32** 60-64

[16] Cruciani S, De Santis V, Feliziani M and Maradei F 2012 Cole-Cole vs Debye Models for the Assesment of Electromagnetic Fields inside Biological Tissues Produced by Wideband EMF Sources *IEEE Electromag. Comp.* 685-688

[17] Stauffer P, Rossetto F, Prakash M, Neuman D, Lee T 2003 Phantom and animal tissues for modeling the electrical properties of human liver *International Journal Of Hyperthermia* **19** 89-101

[18] Nightingale NRV, Goodridge VD, Sheppard RJ, Christie JL 1983 The dielectric properties of the cerebellum, cerebrum and brain stem of mouse brain at radiowave and microwave frequencies *Physics in Medicine and Biology* **28** 897-903

[19] Cuschieri A, Bracken J and Boni L 1999 Initial Experience with Laparoscopic Ultrasound-guided Radiofrequency Thermal Ablation of Hepatic Tumours *Endoscopy* **31** 318-321.

[20] Minami Y and Kudo M 2011 Radiofrequency Ablation of Hepatocellular Carcinoma: a Literature Review *Int J Hepatol.* 1-9

[21] Wright A, Sampson L, Warner T, Mahvi D and Lee F 2005 Radiofrequency versus microwave ablation in a hepatic porcine model *Radiology* **236** 132-139

[22] Wonnell T, Stauffer P and Langberg J 1992 Evaluation of microwave and radio frequency catheter ablation in a myocardium-equivalent phantom model *IEEE Trans. Biomed. Eng.* **39** 1086-1095

[23] Carrafiello G et *al* 2008 Microwave tumor ablation: principles, clinical applications and review preliminary experiences *Int J Surg.* **6** 65-69

[24] Kim Y, Rhim H, Cho O, Koh B and Kim Y 2006 Ontrahepatic recurrence after percutaneous radiofrequency ablation of heat to cellular carcinoma: analysis of the pattern and risk factors *Eur J Radiol*. **59** 432-441

[25] Livraghi T *et al* 2000 Hepatocellular carcinoma: radio-frequency ablation of medium and large lesions *Radiology* **214** 761-768

[26] Lu D *et al* 2003 Influence of large peritumoral vessels on outcome of radiofrequency ablation of liver tumors *J Vasc Interv Radiol* **14** 1267-1274

[27] Yu N, Lu D, Ramen S, Dupuy D, Simon C, Lassman C, Bassam A, Ianniti D and Busuttil R 2006 Hepatocellular Carcinoma: Microwave Ablation with Multiple Straight and Loop Antenna Clusters-Pilot Comparison With Pathologic Findings *Radiology* **239** 269-274

[28] Simon C, Dupuy D and Mayo-Smith W 2005, 'Microwave Ablation: Principles and Applications' *RadioGraphics*, **25** 69-83

[29] Lu D et al. 2001 Effect of Vessel Size on Creation of Hepatic Radiofrequency Lesions in Pigs: Assessment of the "Heat Sink" Effect *American Journal of Roentgenology* **178** 47-51

[30] Yu N, Raman S, Kim Y, Lassman C, Chang X and Lu D 2008 Microwave liver ablation: influence of hepatic vein size on heatsink effect in a porcine model *J Vasc Interv Radiol* **19** 1087-1092

[31] Liang P, Wang Y, Yu X and Dong B 2009 Malignant Liver Tumors: Treatment with Percutaneous Microwave Ablation- Complications among Cohort of 1136 Patients *Radiology* **251:3** 933-940

[32] Lazebnik M, Converse M, Booske J and Hagness S 2006 Ultrawideband temperature-dependent dielectric properties of animal tissue in the microwave frequency range *Physics in Medicine and Biology* **51** 1941-55

[33] Stauffer P, Rossetto F, Prakash M, Neuman D and Lee T 2003 Phantom and animal tissues for modeling the electrical properties of human liver *International Journal Of Hyperthermia* **19** 89-101

[34] Brace C L 2008 Temperature-dependent dielectric properties of liver tissue measured during thermal ablation: toward an improved numerical model *Conf. Proc. IEEE Eng. Med. Biol. Soc* 230–3

[35] Lopresto V, Pinto R, Lovisolo G and Cavagnaro M 2012 Changes in the dielectric properties of *ex vivo* bovine liver during microwave thermal ablation at 2.45 GHz *Physics in Medicine and Biology* **57** 2309-27

[36] Cheung A and Al-Atrash J 1987 Microwave hyperthermia for cancer therapy *IEEE Proceedings* **134** 493–522

[37] Vrbova B and Vrba J 2012 Microwave thermotherapy in cancer treatment: evaluation of homogeneity of SAR distribution *Progress In Electromagnetics Research* **129** 181–195

[38] Wust P et al 2002 Hyperthermia in cancer treatment: hyperthermia in combined treatment of cancer *The Lancet Oncology* **3** 487–497

[39] Colombo R, Da Pozzo L, Salonia A, Rigatti P, Lieb Z, Baniel J, Caldarera E and Pavone-Macaluso M 2003 Multicentric Study Comparing Intravesical Chemotherapy Alone and with Local Microwave Hyperthermia for Prophylaxis of Recurrence of Superficial Transitional Cell Carcinoma *J Clin Oncol* **21** 4270-4276

[40] Issels R 2008 Hyperthermia adds to Chemotherapy *European J Cancer* **44** 2546-2554

[41] Falk M and Issels R 2001 Hyperthermia in oncology *Int. J. Hyperthermia* **17** 1–18

[42] Short J and Turner P 1980 Physical Hyperthermia and Cancer Therapy *Proceedings of the IEEE* **68** 133-142

[43] Rychlik O and Vrba J 2008 Planar spiral applicator for local microwave thermotherapy *14th Conf. Microw. Tech. (COMITE '08)* Apr. 1-3.

[44] Asili M, Green R, Seran S and Topsakal E 2012 A small implantable antenna for medradio and ISM bands *IEEE Antennas Wireless Propag. Lett*. **11** 1683–1685

[45] Kitamura K, Kuwano H, Watanabe M, Nozoe T, Yasuda M, Sumiyoshi K, Saku M and Sugimachi K 1995 Prospective Randomized Study of Hyperthermia Combined with Chemoradiotherapy for Esophageal Carcinoma *J Surg Oncol* **60** 55-58

[46] Sugimachi K, Kitamura K, Baba K, Ikebe M, Morita M, Matsuda H and Kuwano H 1992 Hyperthermia Combined with Chemotherapy and Irridation for Patients with Carcinoma of the Oesophagus –A Prospective Randomized Trial *Int J* **8** 289-295

[47] Ohno S, Tomoda M, Tomisaki S, Kitamura K, Mori M, Maehara Y and Sugimachi K 1997 Improved Surgical Results After Combining Preoperative Hyperthermia with Chemotherapy and Radiotherapy for Patients with Carcinoma of the Rectum *Diseases Colon Rectum* **40** 401-406

[48] Cinti S 2012 The adipose organ at a glance *Disease Models & Mechanisms* **5** 588-594

[49] Frigolet Vazquez-Vela M E, Torres N and Tovar A R 2008 White Adipose Tissue as Endocrine Organ and Its Role in Obesity *Archives of Medical Research* **39** 715-728

[50] Cinti S 2009 Transdifferentiation properties of adipocytes in the adipose organ *American Journal of Physiology-Endocrinology and Metabolism* **297** 977-986

[51] Cannon B and Nedergaard J 2004 Brown adipose tissue: function and physiological significance *Physiol Rev* **84** 277-359

[52] Schulz T et al 2013 Brown-fat Paucity due to impaired BMP signalling induces compesatory browning of white fat *Nature* **495** 379-382

[53] Haas B, Schlinkert P, Mayer P and Eckstein N 2012 Targeting adipose tissue *Diabetology & Metabolic Syndrome* **4** 1-11

[54] Cinti S 2005 The adipose organ *Prostaglandins, Leukot and Essent Fatty Acids* **73** 9-15

[55] Hossain P, Kawar B and Nahas M E 2007 Obesity and diabetes in the developing world - A growing challenge *New England Journal of Medicine* **356** 213-215

[56] Richard D, Monge-Roffarello B, Chechi K, Labbe S M and Turcotte E E 2012 Control and physiological determinants of sympathetically mediated brown adipose tissue thermogenesis *Frontiers in Endocrinology* **3** 36-40

[57] Nedergaard J, Bengtsson T and Cannon B 2007 Unexpected evidence for active brown adipose tissue in adult humans *American Journal of Physiology-Endocrinology and Metabolism* **293** 444-452

[58] Cypess A M, Lehman S, Williams G, Tal I, Rodman D, Goldfine A B, Kuo F C, Palmer E L, Tseng Y H, Doria A, Kolodny G M and Kahn C R 2009 Identification and importance of brown adipose tissue in adult humans *N Engl J Med* **360** 1509-1517

[59] Virtanen K A, Lidell M E, Orava J, Heglind M, Westergren R, Niemi T, Taittonen M, Laine J, Savisto N J, Enerback S and Nuutila P 2009 Functional brown adipose tissue in healthy adults *N Engl J Med* **360** 1518-1525

[60] Muzik O, Mangner T and Granneman J 2012 Assessment of oxidative metabolism in brown fat using PET imaging *Frontiers in endocrinology* **3**

[61] Hu H, Perkins T, Chia J and Gilsanz V 2013 Characterization of human brown adipose tissue by chemical-shift water-fat MRI *AJR. American Journal of Roentgenology* **200**

[62] Lunati E, Marzola P, Nicolato E, Fedrigo M, Villa M and Sbarbati A 1999 *In vivo* quantitative lipidic map of brown adipose tissue by chemical shift imaging at 4.7 tesla *Journal of Lipid Research* **40**

[63] Rothwell N and Stock M 1979 A role for brown adipose tissue in diet-induced thermogenesis *Nature* **281** 31-35

[64] Lee P, Ho K and Greenfield J 2011 Hot fat in a cool man: infrared thermography and brown adipose tissue *Diabetes Obesity & Metabolism* **13** 92-93

[65] Rodrigues D B, Maccarini P F, Salahi S, Colebeck E, Topsakal E, Pereira P, Limao-Vieira P and Stauffer P 2013 Numerical 3D modeling of heat transfer in human tissues for microwave radiometry monitoring of brown fat metabolism. In: *Conference on Energy-Based Treatment of Tissue and Assessment VII,* ed T P Ryan (San Francisco, CA: SPIE)

[66] Stauffer P , Salahi S, Rodrigues D , Topsakal E, Ribeiro T , Prakash A and Maccarini P 2013 Stable microwave radiometry system for long term monitoring of deep tissue temperature. In: *Conference on Energy-Based Treatment of Tissue and Assessment VII,* (San Jose CA, USA: SPIE)

[67] Arunachalam K, Maccarini P, De Luca V, Bardati F, Snow B and Stauffer P 2010 Modeling the detectability of vesicoureteral reflux using microwave radiometry *Phys. Med. Biol* **55** 5417-5435

[68] Dubois L, Sozanski J P, Tessier V, Camart J C, Fabre J J, Pribetich J and Chive M 1996 Temperature control and thermal dosimetry by microwave radiometry in hyperthermia *IEEE Transactions on Microwave Theory and Techniques* **44** 1755-1761

[69] Hand J, Van Leeuwen G, Mizushina S, Van de Kamer J, Maruyama K, Sugiura T, Azzopardi D V and Edwards A D 2001 Monitoring of deep brain temperature in infants using multi-frequency microwave radiometry and thermal modelling *Physics in Medicine and Biology* **46**

[70] Hand J W 2008 Modelling the interaction of electromagnetic fields (10 MHz-10 GHz) with the human body: methods and applications *Physics in Medicine and Biology* **53** 243-286

[71] Casteilla L, Penicaud L, Cousin B and Calise D 2008 Choosing an Adipose Tissue Depot for Sampling *Methods in Molecular Biology* **456** 23-38

[72] Suhling K, Levitt J, Chung P, Kuimova M and Yahioglu G 2012 Flourescence Lifetime Imaging of Molecular Rotors in Living Cells *Journal of Visualized Experiments* **60** 1-5

[73] C. Balanis 2005 Antenna Theory: Analysis and Design John Wiley & Sons, Inc., Hoboken, New Jersey

[74] Klemetsen O Birkelund Y Jacobsen S *et al.* 2011 Design of Medical Radiometer Front-End for Improved Performance *Prog Electromagn Res B Pier B* **27** 289-306